



Contents lists available at ScienceDirect

Earth and Planetary Science Letters

www.elsevier.com/locate/epsl



The solubility of rocks in metamorphic fluids: A model for rock-dominated conditions to upper mantle pressure and temperature

Matthieu E. Galvez^{a,b,*}, Craig E. Manning^c, James A.D. Connolly^b, Douglas Rumble^a

^a Geophysical Laboratory, Carnegie Institution for Science, 5251 Broad Branch Road NW, Washington, DC 20015, USA

^b Department of Earth Sciences (Institute of Geochemistry and Petrology), Swiss Federal Institute of Technology, CH-8092 Zurich, Switzerland

^c Department of Earth, Planetary & Space Sciences, University of California, Los Angeles, CA, USA

ARTICLE INFO

Article history:

Received 8 October 2014

Received in revised form 9 June 2015

Accepted 11 June 2015

Available online xxx

Editor: B. Marty

Keywords:

metasomatism

phase equilibria modeling

COH solutions

dielectrics

polymerization

pH

ABSTRACT

Fluids exert a key control on the mobility of elements at high pressure and temperature in the crust and mantle. However, the prediction of fluid composition and speciation in compositionally complex fluid–rock systems, typically present in subduction zones, has been hampered by multiple challenges. We develop a computational framework to study the role of phase equilibria and complex solid-solutions on aqueous fluid speciation in equilibrium with rocks to 900 °C and 3 GPa. This is accomplished by merging conventional phase-equilibrium modeling involving electrolyte-free molecular fluids, with an electrostatic approach to model solute–solute and solute–solvent interactions in the fluid phase. This framework is applied to constrain the activity ratios, composition of aqueous solutes, and pH of a fluid in equilibrium with a pelite lithology. Two solvent compositions are considered: pure H₂O, and a COH fluid generated by equilibration of H₂O and graphite. In both cases, we find that the pH is alkaline. Disparities between the predicted peralkalinity of our fluid ($([Na] + [K])/[Al] \sim 6$ to 12 and results from independent mineral solubility experiments (~ 2) point to the presence of Na–K–Al–Si polymers representing ca. 60 to 85% of the total K and Al content of the fluid at 600 °C and 2.2 GPa, and to an important fraction of dissolved Ca and Mg not accounted for in present speciation models. The addition of graphite to the system reduces the relative permittivity by ca. 40% at elevated T and low P , triggers the formation of C-bearing anions, and brings the pH closer to neutrality by up to 0.6 units at low T . This ionic C pool represents up to 45 mol% of the fluid ligands at elevated P , and is dominant at low P despite the low ionic strength of the fluid (<0.05). The present study offers new possibilities for exploring redox–pH dependent processes that govern volatile, major and trace element partitioning between rocks and fluids in experimental or natural systems.

© 2015 Elsevier B.V. All rights reserved.

1. Introduction

Metamorphic fluids exert a major control on rheology, reaction kinetics and the transport of heat and matter in the crust and mantle (e.g., Fyfe et al., 1978). Water, in particular, is a powerful solvent for transporting mass on and inside the Earth (e.g., Walther and Helgeson, 1980; Manning, 1994; Ague, 1994), and participating in its long term differentiation. However, metamorphic fluids commonly contain a range of C-bearing species, characterized by no or low permanent dipole moment, that weaken their solvent property (e.g., Deul and Franck, 1991; Walther and Schott, 1988; Walther, 1992). Nevertheless, fluid inclusions rich in CO₂–CH₄–N₂

also contain dissolved solutes, e.g. Na⁺, K⁺, that may precipitate as daughter minerals upon decompression and cooling (e.g., Frezzotti et al., 2011; Ague and Nicolescu, 2014). In addition, specific patterns of element gain-loss or isotopic systematics provide further geochemical evidences for COH fluid-mediated mass transfer, despite their less favorable solvent properties, in a wide range of metamorphic settings (e.g., Bebout and Barton, 1993; Penniston-Dorland and Ferry, 2008; Malvoisin et al., 2012; Galvez et al., 2013a, 2013b; Ague and Nicolescu, 2014).

Despite their importance as metasomatic agents, little is known about dissolution mechanisms, and electrolyte transport in COH fluids (e.g., Evans et al., 2009; Schmidt, 2014). Quantitative prediction of solute mobilization and transport by COH fluids hinges on accurate knowledge of the thermodynamic properties of solvents, solutes, minerals and their solution properties over a wide range of pressure (P) and temperature (T) conditions. Prediction of how rock-forming chemical components are redistributed between mineral and fluids has depended chiefly on indepen-

* Corresponding author at: Department of Earth Sciences (Institute of Geochemistry and Petrology), Swiss Federal Institute of Technology, CH-8092 Zurich, Switzerland.

E-mail addresses: matthieu.galvez@erdw.ethz.ch, matthieu.galvez@gmail.com (M.E. Galvez).

<http://dx.doi.org/10.1016/j.epsl.2015.06.019>

0012-821X/© 2015 Elsevier B.V. All rights reserved.

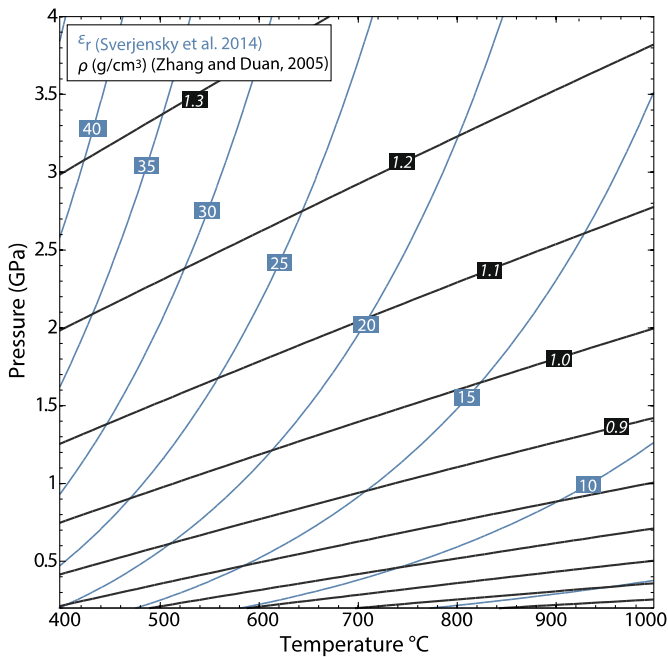


Fig. 1. Contour plot of the static relative permittivity of H₂O (ϵ_r)_{H₂O} (EoS developed by Sverjensky et al., 2014) along with density values from Zhang and Duan (2005). There is an increase of (ϵ_r)_{H₂O} with density increase along isotherms, and with temperature decrease along isochores over the P – T conditions of interest. This can be explained by a combination of bulk and microstructural factors (e.g., Kirkwood, 1939; Yoshii et al., 2001): With increasing temperature along isochores, higher kinetic energies of water molecules induce partial breakage of the hydrogen bond network between water dipoles, progressively annihilating the intermolecular orientational correlation contribution to the overall polarization (for relatively constant dipole moment of individual molecules) and, induce a drop in (ϵ_r)_{H₂O}. With isothermal density increase the tight packing of water molecules and increased hydrogen bonding of H₂O invariably favors an increase of (ϵ_r)_{H₂O} (cf. Appendix A). (For interpretation of the references to color in the figure legends of this paper, the reader is referred to the web version of this article.)

dent models of the thermodynamic properties of aqueous electrolytes (e.g., Helgeson and Kirkham, 1976; Helgeson et al., 1981; Wolery, 1992) and have been hampered by two main challenges. The first challenge is that there have been limitations to assessing the solvent properties of H₂O beyond the P – T range of the commonly used Helgeson–Kirkham–Flowers (HKF) equations of state: In this model, the partial molal Gibbs free energy of hydration $\Delta G_{\text{sol},j}$ of an ion in a solvent follows the Born equation (Helgeson et al., 1981):

$$\Delta G_{\text{sol},j} = \omega_j \left(\frac{1}{\epsilon_r} - 1 \right) \quad (1)$$

where ϵ_r is the relative permittivity of the solvent at P and T , and ω_j is the absolute Born coefficient of the species j . The Born coefficient is an ion-specific function of the ionic charge Z_j , of the effective electrostatic radius (a function of P and T , see Appendix B), and of the vacuum permittivity. The conventional Born coefficient used is defined as $\bar{\omega}_j = \omega_j - |Z_j|\omega_{H^+}$. Expressions for the relative permittivity of pure water, (ϵ_r)_{H₂O}, as a function of density and temperature were long restricted to <0.5 GPa (e.g., Archer and Wang, 1990). However, quantification of (ϵ_r)_{H₂O} has now been extended to ca. 6 GPa, and ca. 1000 °C (Fernandez et al., 1997; Pan et al., 2013; Sverjensky et al., 2014, and Fig. 1). Building on these fundamental advances, this paper explores the new opportunity for integrating petrologic models of rock systems with models of electrolyte chemistry to high P and T .

The second challenge is that there have also been limitations in the extension of the HKF model to geologically complex solvents that contain, in addition to H₂O, species such as CO₂ and CH₄ (e.g.,

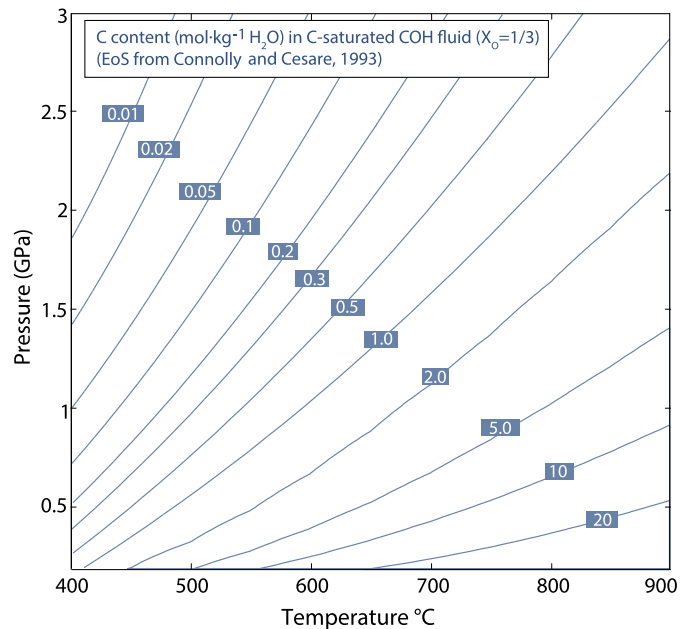


Fig. 2. Contour plot of C molality (mol·kg^{−1} H₂O) in a C-saturated (graphite) COH fluid at $X_0 = 1/3$. The EoS used is from Connolly and Cesare (1993), and it assumes that the solid C phase is perfectly crystalline graphite, refer to Appendix B for details. The C molality spans a large range (10^{-3} to >10 molal) and reaches the highest values at elevated T and lower P as can be expected from the weakly polar nature of H₂O at these conditions, i.e. where (ϵ_r)_{H₂O} is lowest (Fig. 1). The $\log f(\text{O}_2)$ of this fluid ranges between -2.5 (elevated T and low P) and 0 log units (elevated P and low T) below the fayalite–magnetite–quartz (FMQ) equilibrium $\log f(\text{O}_2)$. Interestingly, the solubility of CaCO₃ in pure H₂O (Caciagli and Manning, 2003) displays comparatively limited variations around 0.01 to 0.3 molal in this P – T range, and only equals or exceeds that of C (i.e. graphite here) at the high P and low T conditions typical of the blueschist–lawsonite facies (cf. Fig. 4) where (ϵ_r)_{H₂O} is highest (Fig. 1). This interesting geochemical feature is noteworthy given the dramatically different structure, properties and kinetics of dissolution of these important C-bearing minerals.

Connolly and Cesare, 1993). C concentrations may reach tens of molal in such fluids at elevated T and P and $X_0 = 1/3$ (Fig. 2) ($X_0 = n_{\text{O}}/(n_{\text{O}} + n_{\text{H}})$), and the molar fraction of carbon-bearing species may even exceed that of H₂O during metamorphism of some carbonate lithologies. In such mixed-volatile mixtures, the density and solvent properties, e.g. (ϵ_r)_{mix}, deviate from those of pure H₂O (Fig. 1). Although changes to the ion-solvation energetics (Eq. (1)) can nominally be derived using predictions of the relative permittivity of mixtures of molecules of geological interest (e.g., Looyenga, 1965; Kirkwood, 1939; Wang and Anderko, 2001), this has only rarely been attempted for metamorphic fluids, and, to our knowledge, only to 0.5 GPa (e.g., Walther, 1992; Evans et al., 2006). These two challenges have prevented the application of the HKF model to fluid speciation at lower-crustal and subduction-zone conditions.

An alternative approach to fluid speciation exploits the empirical observations of log–log linear relationships between the dissociation constants of aqueous complex, (ϵ_r)_{H₂O}, and $\rho_{\text{H}_2\text{O}}$ at elevated P and T (e.g., Marshall and Franck, 1981; Manning, 1998; Dolejš and Manning, 2010; Dolejš, 2013) to alleviate the need for values of (ϵ_r)_{H₂O} beyond its range of calibration. However, this method remains largely empirical and does not provide insight into key solvent and solute properties. Moreover, this approach is cumbersome to include with accurate, comprehensive description of the changing compositions of complex mineral solid-solutions that occur in realistic petrological systems over the wide range of P and T relevant to metamorphism, which may include shallow magma-hydrothermal systems, orogenic belts or subduction zones. In contrast, while petrological modeling generally account for com-

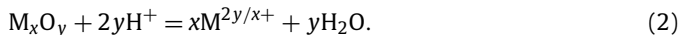
plex solid solution behavior, such models routinely neglect solutes in the coexisting fluid phase.

In the present study, we develop a method that provides insight into the composition and speciation of high-pressure mixed-solvent fluids at equilibrium with assemblages of complex mineral solid solutions. We present the formal basis for this approach, which combines, through general hydrolysis equilibria, the Gibbs free energy of oxide components retrieved from phase equilibrium modeling of solids and molecular fluids, with the Gibbs free energy of dissolved solutes. The latter are derived by an extension of classical electrostatic modeling of COH solution chemistry to extreme P and T , and further constrained by charge balance. The utility of the approach is illustrated using a model metapelite rock at 400–900 °C and 0.2–3.0 GPa, with and without graphite. Our model provisions for the change in ion-solvation energetics by computing the relative permittivity of a COH fluid at $X_O = 1/3$, a reasonable model for a fluid generated by metapelite devolatilization. This approach is designed to isolate and investigate how constituent minerals control the composition and speciation of fluids associated with the rock they form. The results produced are compared with independent experimental data on similar bulk system, and offer a unique window into elusive processes of ionic association at elevated P and T . The outcome is a computational framework within which to investigate the role of metamorphic phase equilibria and complex solid-solutions on the speciation of C-bearing fluids with changing solvent properties to elevated P and T .

2. Computational approach

2.1. Background

The composition of petrological systems can be described by a set of chemical components representing relevant rock- and fluid-forming constituents. For most natural rocks, up to 12 oxide components are adequate to model phase equilibria over a wide range of P and T . The dissolution of rock-forming minerals in aqueous fluids can be represented, in terms of an oxide M_xO_y , by the general hydrolysis reaction:



At equilibrium, the chemical potentials (μ) of the oxide components are linked to the partial molar Gibbs free energy (\bar{g}) of their corresponding dissociated species, here $M^{2y/x+}$, through:

$$\mu(M_xO_y) + 2y \cdot \bar{g}(H^+) = x \cdot \bar{g}(M^{2y/x+}) + y \cdot \mu(H_2O) \quad (3)$$

Equations (2) and (3) make it possible to bring together the two traditional forms of thermodynamic modeling of fluid–rock interaction because they quantitatively relate the chemical potentials of metal oxides, electrolytes and H_2O (Helgeson, 1968). Using oxides in Eqs. (2) and (3) is a particularly convenient way to account for changing mineral solid-solutions over a wide range of P and T in our model. At a given P and T , the chemical potentials of oxide components are obtained by Gibbs energy minimization of a system composed of minerals and of a molecular fluid. The values of μ derived from this model are then employed for purposes of computing the solute speciation. This is valid for closed, rock-dominated system provided the chemical potential retrieved by Gibbs energy minimization (metal oxides and volatile solvent components) are insensitive to the amount of solute in the fluid, which is the case here. Accordingly, the chemical potential of the i^{th} oxide component is the partial derivative of the Gibbs free energy of the solute-free system (G^{sys}) with respect to its number of moles n_i :

$$\mu_i = \left(\partial G^{\text{sys}} / \partial n_i \right)_{T, P, n_k} \quad (4)$$

Table 1

Frequently used symbols.

μ_i	the chemical potential of the i^{th} component
\bar{g}_j	the partial molar Gibbs free energy of the j^{th} aqueous species
\bar{g}_j°	the standard partial molal Gibbs free energy of the j^{th} aqueous species
$(\rho_m)_i$	the molar density of the i^{th} component
\mathcal{P}_i	the polarization of the i^{th} component
$(\epsilon_r)_i$	the (static) relative permittivity of the i^{th} component: $\epsilon_r = \frac{\epsilon}{\epsilon_0}$ with ϵ_0 the vacuum permittivity, ϵ the absolute permittivity
$V_{m,i}$	the molar volume of the i^{th} component
$V_{f,i}$	the volume fraction of the i^{th} component
V_i^*	the critical volume of the i^{th} component
x_i	molar fraction of the i^{th} component
$\gamma_{D,j}$	the activity coefficient (long range ionic interactions) of monovalent ($j = 1$) or divalent ($j = 2$) species
a_i	the activity of the i^{th} component
Ξ_j^i	the log 10 of the ratio among activities of cation i over activity of cation j

and for the j^{th} ion, or neutral complex,

$$\bar{g}_j = \bar{g}_j^\circ + RT \ln a_j \quad (5)$$

where \bar{g}_j° and a_j are, respectively, the standard partial molal Gibbs free energy and activity of the j^{th} solute at P and T (refer to frequently used symbols in Table 1). For aqueous species, we adopt the conventional thermodynamic property $\bar{w}_{H^+} = 0$ leading to $\bar{g}^\circ(H^+) = 0$ (Eq. (1)). It follows that

$$\begin{aligned} \ln \left[\frac{a(M^{2y/x+})}{a(H^+)^{2y/x}} \right] \\ = \frac{1}{RT} [\mu(M_xO_y) - y \cdot \mu(H_2O)/x - \bar{g}^\circ(M^{2y/x+})] \end{aligned} \quad (6)$$

Equation (6) indicates that the ion activity ratio can be derived from the chemical potentials of an appropriate combination of the system's components if \bar{g}_j° at P and T can be determined consistently at a given P and T (Appendix B). Note that for the other species in solution such as hydroxides (e.g., $CaOH^+$, $MgOH^+$ or AlO_2^-), the form of equation (6) is slightly modified with no change in the underlying principle.

In Eq. (6) we use ion activity ratios because, historically, they have been widely used for the depiction of mineral–fluid equilibria (e.g., Bowers et al., 1984). For more compact notation, we define Ξ_a^b as the logarithm in base 10 of the activity ratio of ions a and b . For example, for Eq. (2),

$$\Xi_{H^+}^{M^{2y/x+}} \equiv \log \left[\frac{a(M^{2y/x+})}{a(H^+)^{2y/x}} \right] \quad (7)$$

The standard state for H_2O is taken to be unit activity of the pure phase at any P and T , and for electrolytes it is unit activity of the hypothetical solution of 1 mole of solute in 1000 g of H_2O , referenced to infinite dilution. The \bar{g}° for ions in pure H_2O can be determined using the HKF equations of state (Helgeson et al., 1981) as revised and extended by Tanger and Helgeson (1988) and Shock et al. (1992). Here, $(\epsilon_r)_{H_2O}$ is computed at P and T with an EoS from Sverjensky et al. (2014) with input H_2O densities from Zhang and Duan (2005) (Fig. 1). Various methods have been developed to assess the role of mixed-solvent on fluid speciation: Walther and Helgeson (1980) advocated explicit provision for ionic hydration to rigorously capture the effect of reduced water activity on solute activity, although the method remained qualitative to a large extent (cf. Bowers et al., 1984). Alternatively, the ion solvation energetics can be quantified by adjusting the solvation term of the Gibbs free energy of ions (Eq. (1)) in order to account for changes of dielectric property of the mixed solvent (Dandurand and Schott, 1992;

Walther, 1992). We adopt the second option, which requires computing the relative permittivity of mixed volatile solvents $(\epsilon_r)_{mix}$.

2.2. Relative permittivity of COH fluid

Diluting H₂O by addition of molecular COH species modifies the bulk properties of the solvent, including $(\epsilon_r)_{mix}$ (e.g., Looyenga, 1965; Harvey and Prausnitz, 1987; Walther, 1992). To quantify this effect, the molar fraction of the species that dominate the COH speciation at these elevated T and P , i.e. H₂O, CO₂ and CH₄, are computed with an EoS from Connolly and Cesare (1993). Despite limitations of this molecular model in providing the exact speciation at elevated P (>2 GPa) and low T (<500 °C) where non-ideality increases rapidly (e.g., Aranovich and Newton, 1999) and solutions are very dilute (Fig. 2), these were considered irrelevant for the present purpose of the study.

To compute $(\epsilon_r)_{mix}$ for COH molecular mixtures, one option is to employ mixing rules based on the additivity of the cube roots of the relative permittivity of intermixing species (Landau and Lifshitz, 1960; Looyenga, 1965). This approach has received considerable interest in the geologic community as a means of explaining high T mineral solubility data (e.g., Walther, 1992), by virtue of its success at predicting the dielectric properties of supercritical mixtures of polar and non-polar species (e.g., Deul and Franck, 1991). However, this method was initially derived under the assumption that the relative permittivity of intermixing species are similar (e.g., Looyenga, 1965). As an alternative, we extend to geologic fluids a mixing scheme developed by Harvey and Prausnitz (1987) which has no theoretical restrictions as to the nature and properties of intermixing species, derives $(\epsilon_r)_{mix}$ from estimates of the polarization per unit volume (\mathcal{P}_{mix}) of the mixture as originally proposed [e.g. Eq. (16) in Kirkwood, 1939], and is applicable to non-ideal systems with excess volume of mixing. In this model, $(\epsilon_r)_{mix}$ is given by:

$$(\epsilon_r)_{mix} = \frac{1}{4} (1 + 9\mathcal{P}_{mix} + 3[9\mathcal{P}_{mix}^2 + 2\mathcal{P}_{mix} + 1]^{\frac{1}{2}}) \quad (8)$$

where \mathcal{P}_{mix} is obtained by linear combination of the contribution of each i^{th} component ($V_{f,i}\mathcal{P}_i$) to the polarization of the mixture (e.g., Kirkwood, 1939), $\mathcal{P}_{mix} = \sum_i V_{f,i}\mathcal{P}_i$, and $V_{f,i}$ is the volume fraction of species i in the mixture at P and T of interest. The computation of $V_{f,i}$ uses a method described in Harvey and Prausnitz (1987) and is outlined in Appendix A. The \mathcal{P}_i are functions of the species molar density (ρ_m) _{i} (reciprocal of their molar volume) and of the temperature calibrated to liquid-like densities by Harvey and Lemmon (2005). The polarization of H₂O at P and T is computed using Eq. (8) (Kirkwood, 1939) with input values for $(\epsilon_r)_{\text{H}_2\text{O}}$ from Sverjensky et al. (2014) where H₂O density is from Zhang and Duan (2005). The values of (ρ_m) for CH₄ and CO₂ in the non-ideal mixture are scaled back to the P and T of interest using the relation $(\rho_m)_i = \kappa/v_i^*$, where v_i^* is the critical volume of species i and κ is the critical density of the COH fluid at the P and T of interest computed using an EoS from Connolly and Cesare (1993). It is apparent that the linearity of such mixing scheme requires that the values of \mathcal{P}_i of pure components are unchanged upon mixing of polar and non-polar species. Consequently, this model does not account for the experimental evidences showing the fragmentation of the H-bond network of water by addition of non-polar solutes (e.g., Dubessy et al., 1999; Botti et al., 2008) and it can be anticipated that this approach should slightly overestimate $(\epsilon_r)_{mix}$, although experimental validations are needed. This hypothesis is currently being tested by way of molecular dynamics (MD) simulations of $(\epsilon_r)_{mix}$ in the binary H₂O–CO₂ system to 725 °C and 3 GPa (Mountain and Harvey, submitted). The values of $(\epsilon_r)_{mix}$ obtained with an alternative method to estimate the volume fractions (i.e. by computing

the partial molar volumes of each species at the P – T of interest) and with another mixing rule (Landau and Lifshitz, 1960; Looyenga, 1965, Appendix A) indicate that uncertainties on $(\epsilon_r)_{mix}$ are everywhere within ca. 2–5% in the sub-solidus region (and <16% in the entire P – T range). As a consequence, the anticipated errors on \bar{g}_j° (<3000 J/mol at subsolidus conditions) or on equilibrium constants do not impact the results obtained in this study (Appendix A).

The variation of $(\epsilon_r)_{mix}$ shown in Fig. 3a, c mostly reflects the increasing molar fraction of non-polar C-bearing species in the COH fluid at elevated P and T (Fig. 2). For example, at $P = 1$ GPa and $T = 700$ °C, where the concentration of C in C-saturated COH fluid at $X_O = 1/3$ is ca. 2 molal, $(\epsilon_r)_{mix}/(\epsilon_r)_{\text{H}_2\text{O}} \sim 0.9$. The values of $(\epsilon_r)_{mix}$ are used to compute \bar{g}° in Eq. (6) from Eq. (1). That is, the energetics of ions in going from a pure H₂O fluid to a COH mixture, i.e. the dielectric correction to the solvation term, Eq. (1) (Appendix B), is incorporated to the standard state Gibbs free energy of the ions in the mixed-solvent. Accordingly, the modified standard state corresponds to unit activity of the solution of 1 mol of solute in 1000 g of the mixed solvent composed of uncharged COH molecular species and referenced to infinite dilution. As a result, the activity coefficients of ions only include non-ideality arising from long range ionic interaction (Helgeson et al., 1981), and are described below by the Davies equation (other details of the computational strategy and conventions are outlined in Appendix B). The values of $(\epsilon_r)_{mix}$ can be used, in particular, to show how the values of pH at acid–base neutrality in the mixture ($\text{pH}_w^{\text{mix}} - \text{i.e. } a(\text{H}^+) = a(\text{OH}^-) - \text{increase in response to the presence of additional COH molecular species (Fig. 3b).$

3. Applications to a model subaluminous pelite system

3.1. Description of the models and main assumptions

We consider two models involving minerals in the Na₂O–CaO–K₂O–FeO–MgO–Al₂O₃–SiO₂–O–H±C system, in which a fluid is equilibrated with an average sub-aluminous pelite, with slightly reduced CaO content (e.g., Caddick and Thompson, 2008). The ubiquity of graphitic material in pelitic rocks makes it a particularly useful lithology to evaluate the role of C on fluid speciation at depth. Model #1 is carbon free and assumes that the fluid is pure H₂O. Model #2 is carbon bearing and assumes a C-saturated COH fluid with $X_O = 1/3$ (and the molecular species H₂O, CO₂, CO, CH₄, H₂ and O₂; Connolly and Cesare, 1993). Equilibrium phase relations are computed at 400–900 °C and 0.2–3.0 GPa. The fluid phase is considered to be present in excess over the entire P – T range. The bulk rock composition is constant except for H₂O, which varies with the change in phase assemblage as required by the assumption of fluid saturation. Melting was not considered in these computations which use end-member thermodynamic data from Holland and Powell (1998, 2002 revision). Mineral solid solution models are listed in Appendix C.

The P – T section for the metapelite bulk composition is shown in Fig. 4. The position of the H₂O-saturated solidus is shown in Fig. 4 to highlight the P – T region where the calculations are metastable with respect to the presence of a silicate liquid in model #1 (model listed in Appendix C). The solidus would be at a marginally higher T at any P in the presence of a COH fluid (model #2). No carbonate minerals are predicted to be stable at any of the P – T conditions investigated (see also Fig. 2). The bulk H₂O content is illustrated in Fig. 4 using the contours of water weight fraction in the rock at equilibrium (model #1), and the carbon concentration in the fluid phase that is required for graphite saturation (model #2) is shown in Fig. 2.

In order to link the phase relations depicted in Fig. 4 to the charge balance and chemistry of the fluid phase, we assume that

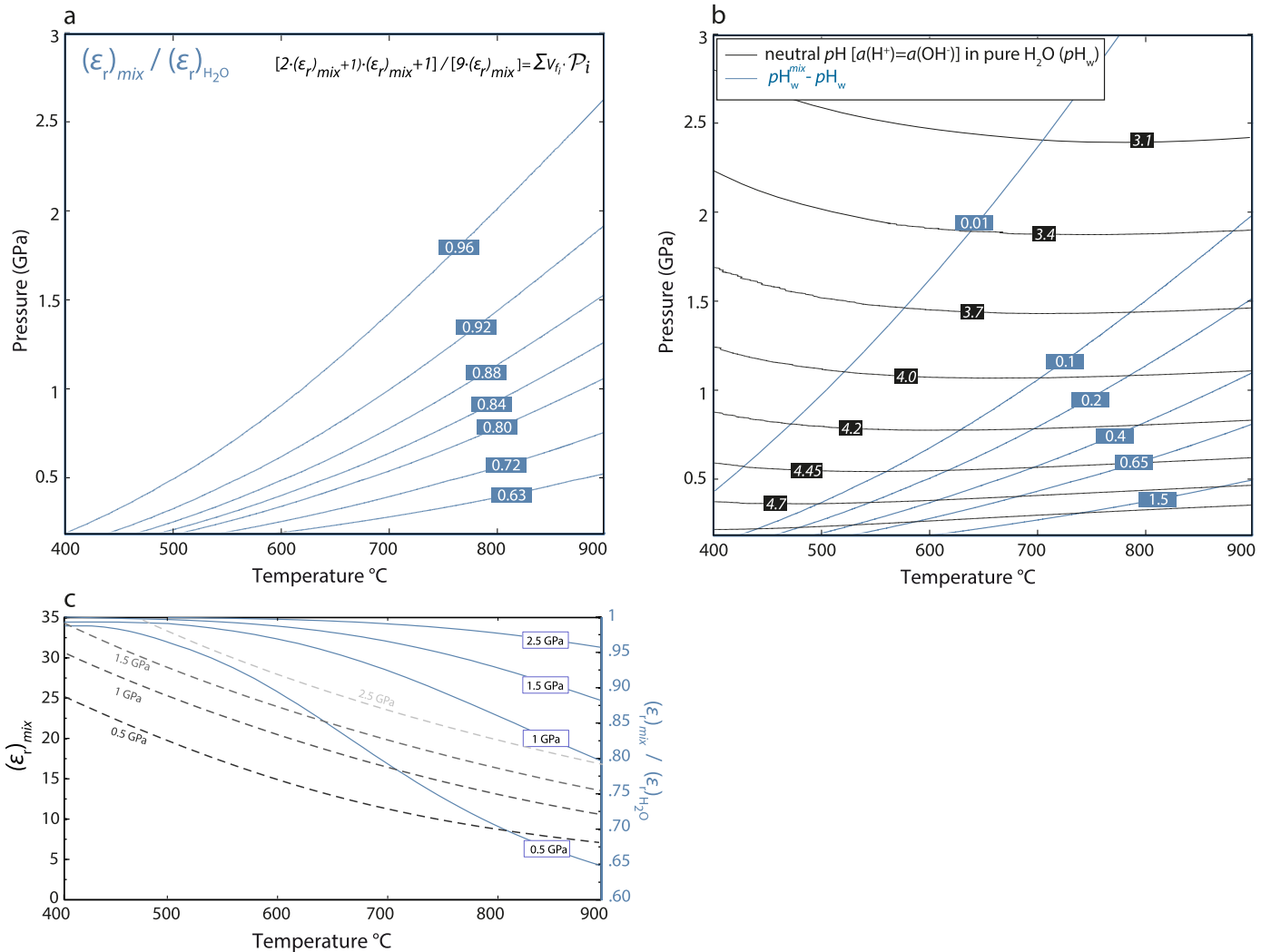


Fig. 3. a. Ratio of the relative permittivity of a COH fluid $(\epsilon_r)_{mix}$ to that of pure H₂O $(\epsilon_r)_{H_2O}$. $(\epsilon_r)_{mix}$ has been estimated using the EoS from Connolly and Cesare (1993) to retrieve molar fraction of the H₂O, CO₂ and CH₄ species. The relative permittivity of non-polar COH species (no permanent dipole moment) is from Harvey and Lemmon (2005), the values of $(\epsilon_r)_{H_2O}$ are from Sverjensky et al. (2014) and the mixing rule to compute the polarization of the COH fluid is from Harvey and Prausnitz (1987) (refer to Appendix A for uncertainties associated to these estimates). Profiles at 0.5, 1, 1.5 and 2.5 GPa are provided in (c) showing the non-linear up-T evolution of $(\epsilon_r)_{mix}$ reflecting increasing dissolution of C. Similar calculation for the simple binary H₂O–CO₂ system (EoS from Holland and Powell, 1991, 1998, 2003) is provided as indication in Supplementary Material, SOM F1. b. Contour plot of the pH (pH_w) of pure H₂O (black) at neutrality as defined by $a(H^+) = a(OH^-)$, i.e. $pH_w = pK_w/2$. The dissociation constant of water is from Bandura and Lvov (2006). Also shown is the relative change of pH at neutrality in a molecular mixture $(pH_w^{mix} = (pK_w^{mix} - \log(a(H_2O)))/2)$ characterized by $a(H_2O) < 1$ and a reduced water dissociation constant K_w^{mix} (see also Section 4.3, Appendix B and Walther, 1992, for details). Thus, a positive value for the difference $pH_w^{mix} - pH_w$ (blue line) indicates that neutrality in the molecular mixture corresponds to higher pH values than pH_w . The dielectric effect on the increase of pK_w^{mix} is largely dominant over the term dependent on $a(H_2O)$.

the non-electrolyte fluid–rock equilibria are independent of the electrolyte chemistry of the fluid (see Section 2.1). Our modeling is essentially designed to isolate and investigate how constituent minerals contribute to and control the composition and speciation of fluids associated with the rock they form. Other factors – e.g., halogen concentration, which may be internally or externally controlled (e.g., Yardley and Graham, 2002) – can be included but are outside the scope of the present work (Galvez et al., in preparation). Thermochemical data for aqueous species used in this study are those compiled and revised by Sverjensky et al. (2014) unless otherwise stated (see also Appendix B).

3.2. Electrolyte activity ratios

Fig. 5 is contoured with isolines of $\mathcal{E}_{H^+}^{Na^+}$ and $\mathcal{E}_{H^+}^{K^+}$ in pure H₂O (model #1, Fig. 5a and c) and in graphite-saturated H₂O (model #2, Fig. 5b and d), in equilibrium with the model pelite (similar plots

for the ratio $\mathcal{E}_{Mg^{2+}}^{Ca^{2+}}$ can be found in SOM Fig. 2a, b). It illustrates the response of the electrolyte activities in the fluid to variations in P , T and mineral assemblages regardless of fluid speciation. Also shown are three P – T paths: path 1, a model path corresponding to the top of a subducting slab (Syracuse et al., 2010); path 2, isobaric heating in the middle crust; path 3, a model exhumation path from high pressure conditions. Fig. 5a shows that the values of $\mathcal{E}_{H^+}^{Na^+}$ display limited sensitivity to T ; they are within ca. 2 log units (3.6–5.3) over the entire P – T interval. These values are similar to previous calculations involving stoichiometric minerals (Bowers et al., 1984) at comparable conditions: Bowers et al. (1984) obtain $\mathcal{E}_{H^+}^{Na^+} \sim 4.7$ at albite–sillimanite–quartz equilibrium (600 °C, 0.5 GPa), as compared to ~ 4.2 here (Fig. 5a), consistent with the reduced activity of the albite end-member in plagioclase in the present calculations. Similarly, the \mathcal{E} values are in agreement (within ca. 0.1 log unit) with those found by Manning (1998) at the blueschist–eclogite transition, in spite of his different com-

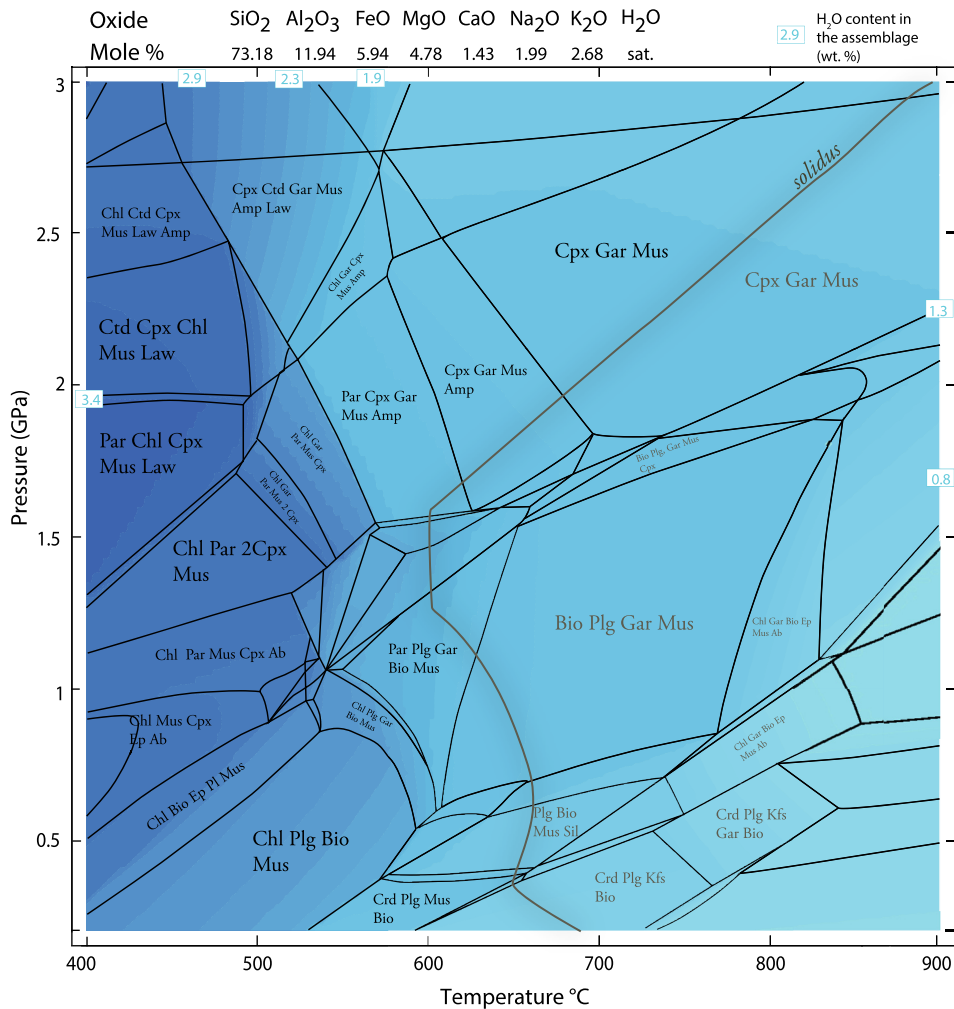
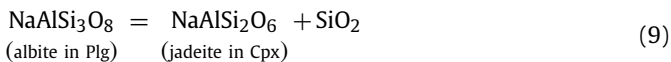


Fig. 4. P – T section in the NCKFMASH system for a model pelite indicating the location of the main mineral assemblages. Blue shading in the background indicates the isopleth of the H_2O content present in the rock at equilibrium (wt%). For example, the 400–600 °C and 1–3 GPa interval corresponds to the blueschist–eclogite transition, characterized by significant H_2O loss by the mineral assemblage (>3.4 wt% at blueschist conditions to ca. 1.5 wt% H_2O at eclogite conditions) in response to continuous devolatilization of hydrous-phases, *i.e.* lawsonite, chloritoid, chlorite and glaucophane. Black contours delineate distinct mineralogical phase fields and sub-solidus assemblages are indicated in black. Super-solidus assemblages, metastable with respect to a melt phase, are indicated in dark green. The position of the wet-solidus is also indicated. Starting composition is indicated above the figure (adapted from Caddick and Thompson, 2008) and solution models used can be found in Appendix C.

putational approach and restriction to the simple NMASH system (Table 2).

A prominent feature of Fig. 5a, b is the maximum reached by $\mathcal{E}_{\text{H}^+}^{\text{Na}^+}$ along the equilibrium,



Irrespective of T , an isothermal increase in P leads to an increase of $\mathcal{E}_{\text{H}^+}^{\text{Na}^+}$ to a maximum of ~ 5.2 in the region of Eq. (9), followed by a decline to values similar to those at low P . This feature and the more subtle variations in $\partial \mathcal{E}_{\text{H}^+}^{\text{Na}^+} / \partial P$ unrelated to Eq. (9) are predominantly controlled by the variation in mode and partial molar volume (v) of Na_2O -bearing phases owing to the relation:

$$\left(\frac{\partial \mu_i}{\partial P} \right)_{T, n_k (k \neq i)} = \left(\frac{\partial V^{\text{sys}}}{\partial n_i} \right)_{P, T, n_k (k \neq i)} \quad (10)$$

where V^{sys} designates total volume of the fluid–rock system. At $P < 1$ GPa and 500 °C, the main Na_2O bearing phases are plagioclase ($v_{\text{albite}} \sim 100 \text{ cm}^3/\text{mol}$ at 1 GPa and 500 °C) and white mica ($v_{\text{white mica}} \sim 139 \text{ cm}^3/\text{mol}$ at 0.9 GPa and 500 °C). There is an increase of white mica modal abundance as P rises from 0.2 GPa

(22 wt%) to 0.9 GPa (33 wt% white mica), along with a slight increase of Na_2O partitioning in this phase with increasing pressure (from 13.5 to 13.8 wt% $\text{Na}_2\text{O}_{\text{tot}}$). This feature governs the steady increase in $\mathcal{E}_{\text{H}^+}^{\text{Na}^+}$ over this P – T interval. Conversely, for P greater than ~ 1 GPa, the lower molar volume of jadeitic clinopyroxene ($\sim 60.6 \text{ cm}^3/\text{mol}$ at 1 GPa and 400 °C) coupled with an up- P increase in its modal abundance leads to the inversion of $\partial \mathcal{E}_{\text{H}^+}^{\text{Na}^+} / \partial P$ to negative values starting at $P \sim 1$ GPa at 400 °C (Eq. (9)) and continuing to higher P (and T) (Figs. 4 and 5). Thus, the $\mathcal{E}_{\text{H}^+}^{\text{Na}^+}$ isolines are chiefly controlled by the isothermal relative evolution of clinopyroxene, plagioclase and white mica solid solution composition.

Values of $\mathcal{E}_{\text{H}^+}^{\text{K}^+}$ (Fig. 5c) display a limited spread (2.6–4.2) over the examined P – T space. Both the variations of this ratio and the isoline slopes show a complex dependence on P , T and phase assemblages. These are tied to white mica and biotite compositions as these are the only major K_2O -bearing phases over most of the P – T range (K-feldspars is only present at $P < 0.7$ GPa and $T > 700$ °C). As with $\mathcal{E}_{\text{H}^+}^{\text{Na}^+}$, values of $\mathcal{E}_{\text{H}^+}^{\text{K}^+}$ show a broad ridge in the vicinity of Eq. (9). At P greater than this equilibrium, isolines generally have positive dP/dT values, reaching ca. +10 $\text{MPa } ^\circ\text{C}^{-1}$ in the eclogite facies, and $\mathcal{E}_{\text{H}^+}^{\text{K}^+}$ increases slightly from 3 to 3.8

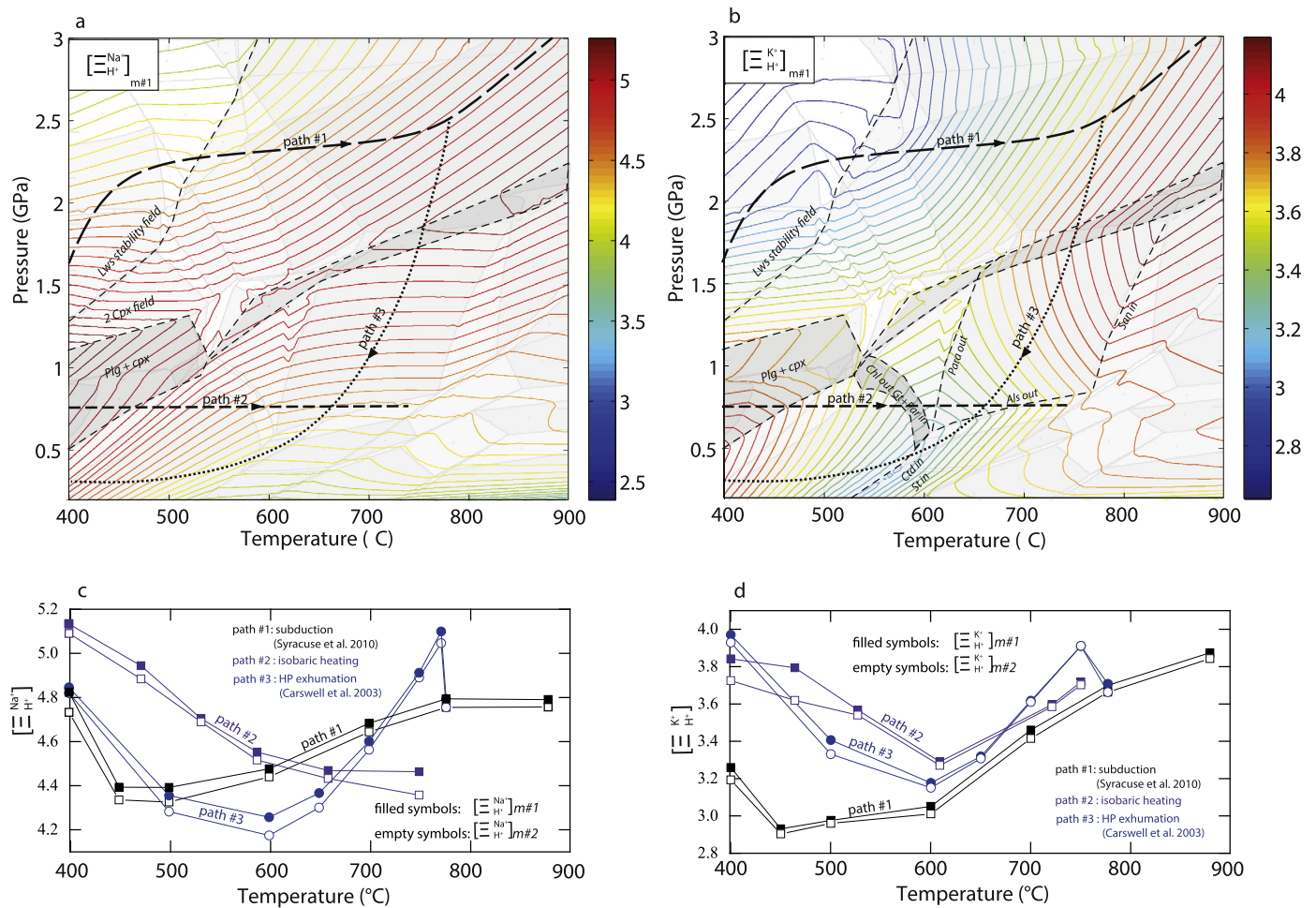


Fig. 5. Contours of activity ratio for selected cations at equilibrium with a devolatilizing metapelite (Fig. 4) for model #1 (pure H₂O) and model #2 (C-saturated COH fluid, $X_0 = 1/3$): **a.** $\mathcal{E}_{\text{H}^+}^{\text{Na}^+}$ for model #1. It shows the P dependence of $\mathcal{E}_{\text{H}^+}^{\text{Na}^+}$ ratio, reaching a maximum along equilibrium (11). It also shows the T dependence of $\mathcal{E}_{\text{H}^+}^{\text{Na}^+}$ isolines slopes (see text for details). **b.** $\mathcal{E}_{\text{H}^+}^{\text{K}^+}$ for model #1. The low P domain of biotite–muscovite costability is the prominent feature. In addition, profiles along a subduction (path #1), isobaric heating (path #2), and exhumation (path #3, Carswell et al., 2003) paths for the ratio $\mathcal{E}_{\text{H}^+}^{\text{Na}^+}$ (model #1, filled symbols and model #2, empty symbols) (**c**) and the ratio $\mathcal{E}_{\text{H}^+}^{\text{K}^+}$ (**d**) are indicated. Note that some high- T portions of paths #2 and #3 cross the solidus and would require fluid addition (ca. 2 wt%) to maintain equilibrium. This shows the negligible effect of the addition of C on the values and shape of the standard-state variables $\mathcal{E}_{\text{H}^+}^{\text{Na}^+}$ and $\mathcal{E}_{\text{H}^+}^{\text{K}^+}$.

along path 1. At low P , $\mathcal{E}_{\text{H}^+}^{\text{K}^+}$ exhibits a minimum of 3.3 between 500 and 600 °C at $P < 0.5$ GPa in the stability field of Bio + Mus ± Par (Fig. 4).

This valley is characterized by a minimum of the K₂O molar fraction in the muscovite ($X(\text{K}_2\text{O}^{\text{A site}}) = \text{K}_2\text{O}/(\text{K}_2\text{O} + \text{CaO} + \text{Na}_2\text{O})^{\text{A site}}$) of ~ 0.51 at 590 °C and 0.5 GPa (with 48 wt% of K₂O_{tot} in white mica, 52 wt% of K₂O_{tot} in biotite) compared to ~ 0.85 at 690 °C (with 22 wt% of K₂O_{tot} in white mica, 78 wt% of K₂O_{tot} in biotite). Simultaneously, biotite abundance in the assemblage increases from ~ 0.8 wt% at 400 °C and 0.5 GPa, to a maximum of ~ 29 wt% at 650 °C, and then decreases to ~ 23 wt% at 690 °C where white mica in the assemblage is replaced by K-feldspar. These variations highlight that entropy changes of assemblages of mineral solid solutions exhibit subtle variations with temperature, leading to isobaric fluctuations of $\partial \mathcal{E}_{\text{H}^+}^{\text{Na}^+}/\partial T$ and $\partial \mathcal{E}_{\text{H}^+}^{\text{K}^+}/\partial T$ owing to:

$$\left(\frac{\partial \mu_i}{\partial T}\right)_{P, n_k (k \neq i)} = \left(\frac{\partial S^{\text{sys}}}{\partial n_i}\right)_{P, T, n_k (k \neq i)} \quad (11)$$

where S^{sys} designates the total entropy of the fluid–rock system.

In general, the limited spread of values for the two variables $\mathcal{E}_{\text{H}^+}^{\text{Na}^+}$ and $\mathcal{E}_{\text{H}^+}^{\text{K}^+}$ at elevated P and T is remarkable, and suggests that any parameter (e.g. pH, see Section 4.3) or process showing

strong dependence on $\mathcal{E}_{\text{H}^+}^{\text{Na}^+}$ and/or $\mathcal{E}_{\text{H}^+}^{\text{K}^+}$ may exhibit the same characteristics. However, greater variation in these activity ratios may be expected when additional ligands and controls on fluid composition (e.g. presence of chloride) are considered.

The P – T variations in the activity ratios differ only slightly between models #1 and #2. At low P and low T , the values of $\mathcal{E}_{\text{H}^+}^{\text{K}^+}$ and $\mathcal{E}_{\text{H}^+}^{\text{Na}^+}$ obtained with model #2 decrease by only about 5% (Fig. 5c, d) in response to a combination of three factors [Eq. (6)]:

(1) Modifications in the stable phase assemblages. For example, at 450 °C and 0.5 GPa, the modes of biotite and chlorite are respectively 6 and 13.5 wt% in model #1, but 5 and 13.8 wt% in model #2 in response to lowered $a(\text{H}_2\text{O})$. In addition, clinopyroxene becomes stable at lower P in model #2.

(2) Change in H₂O chemical potential with added C components.

(3) Modification of the solvent properties of the fluid in the presence of non-polar species.

4. Discussion

4.1. Prediction of solute concentrations

Combining the activity ratios computed above with activity models for solutes and charge balance allows prediction of the

Table 2

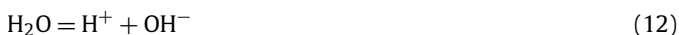
Computation results. The ionic strength (I), activity coefficient of monovalent species ($\gamma_{D,1}$), of divalent species ($\gamma_{D,2}$), the pH, the molality of elements and several geochemical indicators (e.g. the ratio $([K]+[Na])/[Al]$) are provided. These are compared to experimental studies (Wohlert et al., 2011 and Spandler et al., 2007) or modeling work (Manning, 1998).

T (°C)	600			600			600			600				
P (GPa)	1.2			2			2.25			2				
Reference	(a)		this study	(a)		this study	(a)		this study	(b)		this study	(c)	
Chemical system	APQ	APQ	JPQ	JPQ	JPQ	JPQ	JPQ	JPQ	JPQ	NMASH	NCKFMASH	NCKFMASH	NCKFMASH	this study
<i>Calculation results</i>														
I		0.06	Δ		0.16	Δ		0.16	Δ		0.17			0.17
$\gamma_{D,1}$		0.73			0.70			0.71			0.55			0.55
$\gamma_{D,2}$											0.09			0.09
pH		6.20			5.75			5.52			5.67			5.50
<i>Elemental abundance</i>														
log[Na]	-0.67	-1.18	69	-0.43	-0.76	54	-0.46	-0.77	51	-0.40	-0.87	-0.83	-0.87	8
log[Al]	-0.81	-1.80	90	-0.74	-1.79	91	-0.84	-1.87	91	-1.80	-1.44	-0.99	-1.54	72
log[Si]	-0.02	-0.37	55	0.14	-0.22	57	0.10	-0.19	49	-0.20	-0.22	0.03	-0.19	41
log[K]											-1.56	-1.30	-1.65	56
log[Ca]											-5.21	-1.43	-4.97	100
log[Mg]										-6.00	-5.37	n.a.	-5.12	
[Si]/[Al]	6.19	27.19		7.55	37.22		8.83	48.46		39.81	16.75	10.57	22.25	
$([K]+[Na])/[Al]$	1.39	4.14		2.05	10.77		2.43	12.61		25.12	4.46	1.94	5.50	
[Na]/[Si]	0.22	0.15		0.27	0.29		0.27	0.26		0.63	0.22	0.14	0.21	
[Na]/[K]											4.87	2.95	6.11	
[K]/[Al]											0.76	0.49	0.77	

Notes: The chemical systems are referred to as APQ for Albite-Paragonite-Quartz, JPQ for Jadeite-Paragonite-Quartz (Wohlert et al., 2011). The values are computed here with bulk composition $\text{SiO}_2(\text{sat})$, $\text{Al}_2\text{O}_3/\text{Na}_2\text{O} = 1.3$ (molar basis) to produce the Alb-Par-Q or Jd-Par-Q phase assemblages consistent with the experimental system (Wohlert et al., 2011). The Ab \rightarrow Jd + Q transition is predicted to occur at ca. 1.5 GPa at 600 °C. The bulk fluid composition reported by Spandler et al. (2007) has been recalculated, in molal concentration scale, from their Table 5, sample PFI3. The uncertainties on [X] values due to uncertainties in mineral properties is estimated to be ca. $\pm 30\%$ of the [Na], [K] and [Al] values, and ca. 10% of [Si] values, a conservative estimate. Uncertainties on pH predictions are below 0.1 pH unit. See Appendix B for further details. The column marked Δ represents the missing quantity of element X, i.e. [X], compared to reported experimental values (in %, on a molal basis). The complex $\text{KAlO}_{2,\text{aq}}$ is included in the calculations leading to the results reported here.

References: (a) Wohlert et al. (2011), (b) Manning (1998), (c) Spandler et al. (2007).

distribution of mass between the rock and the fluid phase implied in each model. We adopt an initial set of ten ionic species (cations Na^+ , K^+ , Ca^{2+} , Mg^{2+} , CaOH^+ , MgOH^+ , H^+ and anions AlO_2^- , OH^-) and seven neutral species ($\text{SiO}_{2,\text{aq}}$, $\text{Si}_2\text{O}_{4,\text{aq}}$, NaOH_{aq} , $\text{NaHSiO}_{3,\text{aq}}$, $\text{NaAlO}_{2,\text{aq}}$, KOH_{aq} , $\text{HAlO}_{2,\text{aq}}$), where $\text{SiO}_{2,\text{aq}}$ and $\text{Si}_2\text{O}_{4,\text{aq}}$ respectively denote the silica monomer and dimer. Each species is linked to an equation of a form similar to Eq. (6). We assume that silica occurs only as neutral species due to uncertainties in the accuracy of thermochemical data of HSiO_3^- over the P - T range investigated. However, as a check, the calculations were repeated including HSiO_3^- , for which data are from Sverjensky et al. (1997). We also neglected the positively charged Al species Al^{3+} , AlOH^{2+} , and AlO^+ because trial calculations revealed neutral to alkaline pH values at which these species had relatively low concentrations. Activity coefficients of charged species in the fluid ($\gamma_{D,j}$) were calculated using the Davies equation (Appendix B). Activity coefficients for neutral complexes were assumed equal to 1. The equilibrium constant K_w of the water dissociation (ionization) reaction



is taken from the most recent estimate proposed by Bandura and Lvov (2006) in model #1. In model #2, it is modified (K_w^{mix}) using our estimates of $(\varepsilon_r)_{\text{mix}}$ to account for its deviation from K_w in pure water [e.g., Fig. 3b and Appendix B]. Charge balance provides the last constraint on the system:

$$\sum_j Z_j m_j = 0 \quad (13)$$

where Z_j is the ionic charge. Under these conditions, a system of 12 non-linear equations for model #1, and 17 equations for model #2, can be iteratively solved for H^+ activity, as well as for each electrolyte molalities in the fluid (Appendix B).

The resulting values for the molalities of a range of elements are reported for selected P and T in Table 2. Element abundance are found in the order $[\text{Si}] > [\text{Na}]$, $[\text{Al}] \approx [\text{K}] > [\text{Ca}] > [\text{Mg}]$, and the ionic strength (I) varies between 10^{-3} (low P) and 1 over most of the P - T space investigated, with a mean ca. $I = 0.15$. The steady decrease in $[\text{Ca}]/[\text{Mg}]$ (and $\varepsilon_{\text{Mg}^{2+}}^{\text{Ca}^{2+}}$) with rising T indicates that elevated [Ca] relative to [Mg] may be characteristic of low P - T environments, whereas higher [Mg] relative to [Ca] occurs over a broad range of high metamorphic P and T (SOM Fig. 2). Along with increasing [Si] with rising P - T , our model shows that Si is increasingly partitioned in the dimer with rising T and decreasing P (SOM Fig. 3), and attain equipartition between Si-monomers and Si-dimers at 700 °C and 1 GPa (see also Manning et al., 2010). Thus, the fraction of Si-dimer tracks the decreasing values of $(\varepsilon_r)_{\text{H}_2\text{O}}$ (Fig. 1), and our results are in qualitative conformity with the numerous field evidence for preferential mobility of Si, alkali (Na, K) or Al in crustal or slab fluids (e.g., Bebout and Barton, 1993; Penniston-Dorland and Ferry, 2008; Bucholz and Ague, 2010; Galvez et al., 2013b), sometimes precipitated in kyanite + quartz (\pm omphacite) (e.g. Widmer and Thompson, 2001; Bucholz and Ague, 2010) or albite + quartz veins (e.g., Bucholz and Ague, 2010).

4.2. Comparison between predicted and experimental determinations of fluid composition

The comparison of our predictions with experimental studies can provide valuable information about solute associations not yet considered in current thermochemical modeling of fluid speciation. The thermochemical data for aqueous silica (Sverjensky et al., 2014) accurately reproduce quartz solubility and silica speciation at elevated P and T (Manning, 1994; Zotov and Keppler, 2000; Mysen, 2010). However, uncertainties in the data for HSiO_3^- prevent rigorous assessment of the contribution of dissolved silica to

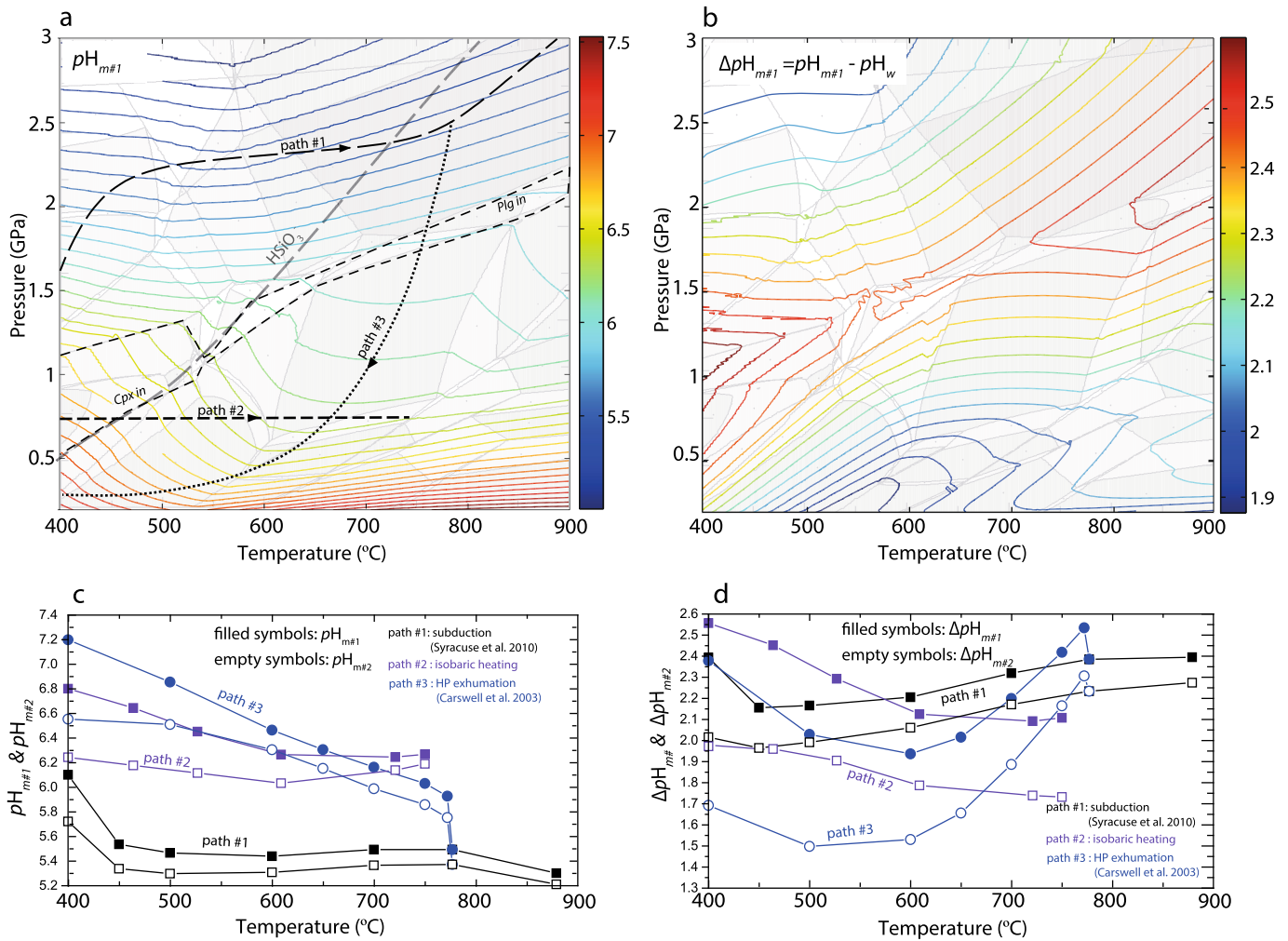


Fig. 6. a. Equilibrium pH computed by solving Eqs. (6), (12), (13) for the modeled metapelite in model #1 (filled symbols). b. This panel shows the pH difference $\Delta pH_{m\#1} = pH_{m\#1} - pH_w$. It is a measure of the *alkalinity* (or acidity) of the equilibrium fluid relative to neutrality pH_w (Fig. 3). The values show a broad maximum at the location of Eq. (9), and decrease at P - T conditions further away from this equilibrium. The difference $\Delta pH_{m\#2} = pH_{m\#2} - pH_w^{mix}$ is the *alkalinity* of the equilibrium fluid (model #2), computed relative to acid-base neutrality in the mixture pH_w^{mix} (refer to Fig. 3, text and Appendix B for details). The profile of $pH_{m\#1}$ (filled symbols) and $pH_{m\#2}$ (empty symbols) and $\Delta pH_{m\#1}$ and $\Delta pH_{m\#2}$ are reproduced along three P - T paths in c and d respectively. The trends show that addition of C affects the pH in a complex fashion.

the overall charge balance of the fluid and introduce some uncertainties on the total Si solubility at these alkaline conditions. At low T and elevated P , neutral silica monomers and polymers are most probably metastable, to a certain extent, with respect to $HSiO_3^-$, as revealed by repeating the calculations using the available thermochemical data for this anion. Similarly, the data for $HAIO_{2,aq}$ and AlO_2^- are from Sverjensky et al. (2014), and those of $KAlO_{2,aq}$ from Pokrovskii and Helgeson (1997). Using these species, Sverjensky et al. (2014) report good reproducibility of corundum solubility in a wide range of P - T conditions, at both neutral (e.g., Tropper and Manning, 2007), and alkaline conditions (i.e. Wohlers and Manning, 2009). Regardless, our prediction for the fluid peralkalinity at 600 °C and 2.2 GPa, ca. $([Na] + [K])/[Al] \sim 12$, or for the $[Si]/[Al]$ ratio, ca. 50, remain relatively remote from experimental measurements at similar conditions, e.g. $([Na] + [K])/[Al] \sim 2$, and $[Si]/[Al] \sim 10$, by Spandler et al. (2007). Including a K-Al complex $KAlO_{2,aq}$ to model #1 somewhat reduces the difference between our predictions, e.g. $([Na] + [K])/[Al] \sim 6$, $[Si]/[Al] \sim 20$, and the experimental values derived from Spandler et al. (2007), but a substantial discrepancy that exceeds uncertainties due to mineral or solute thermochemical properties persists, pointing to the existence of alkali-aluminosilicate polymers not accounted for in the present speciation. These additional K-Al, K-Si and K-Al-Si species represent an important fraction of [Al] and [K], i.e. 60 to 85% of

their total solubility, at 600 °C and 2.2 GPa (Table 2). Similarly, solutes are needed to explain the discrepancies observed for [Ca] and [Mg]. Notably, this appears to be a feature characteristic of high P fluids. For example, Pak et al. (2003) determined the solubility of the pelitic assemblage albite + K feldspar + andalusite + quartz in aqueous chloride solutions at 600 and 650 °C, 0.2 GPa, and found it unnecessary to invoke additional species to K-Al and K-Si complexes to explain their results.

Wohlers et al. (2011) investigated the solubility of albite/jadeite-paragonite-quartz in H_2O at 500 and 600 °C and a range of P . Applying our method to this simplified system returns values for both [Na] and [Al] that are underestimated (model #1) by 0.17 ± 0.02 molal, and [Si] by 0.55 ± 0.05 molal at all conditions (this deficit represents ca. 50% of [Na], [Si] and 90% of [Al], Table 2).

4.3. Rock control on pH variations

The pH in model #1 is alkaline over the investigated P - T range (Fig. 6a), with values up to ca. 2.6 log units over neutral pH in the vicinity of equilibrium (9) (Fig. 6b). The *alkalinity* ($\Delta pH_{m\#1}$) of the fluid is the difference between buffered pH ($pH_{m\#1}$) and acid-base neutrality [i.e. pH_w corresponding to the condition $a(H^+) = a(OH^-)$, Eq. (12), and Fig. 3b], thus $\Delta pH_{m\#1} = pH_{m\#1} - pH_w$. As predicted based on alkali activity ratios (Fig. 5), pH is relatively

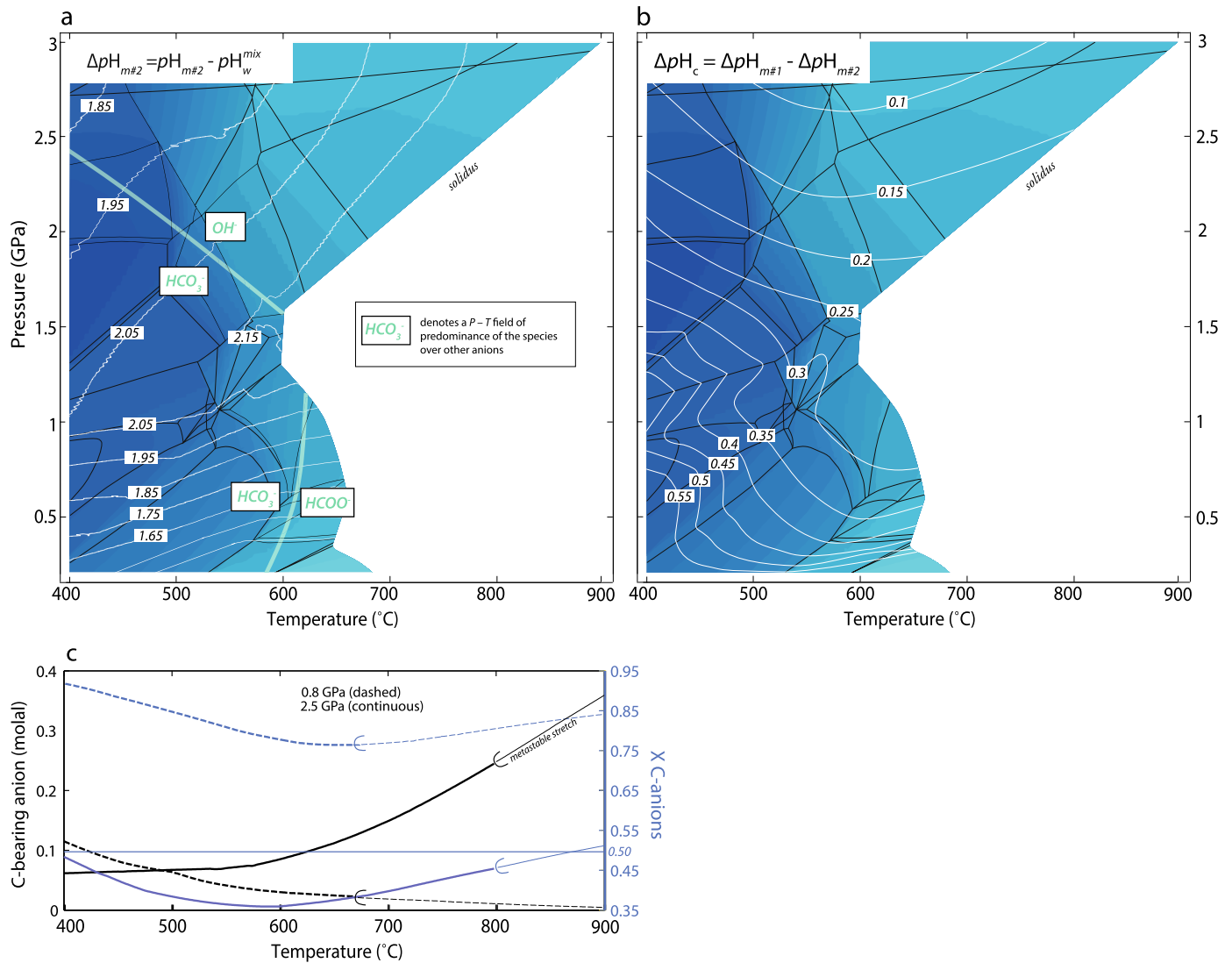


Fig. 7. a. Contours of $\Delta pH_{m\#2}$. The predominant ligands are indicated along with their P - T field of predominance (thick pale-green line). The water content of the rock (blue shading) and the main mineral stability fields (black lines) are also indicated. Details can be found in Fig. 4. b. Contours of $\Delta pH_c = \Delta pH_{m\#1} - \Delta pH_{m\#2}$, a measure for the relative alkalinity of the fluid between model #1 (pure H_2O) and model #2 (COH fluid at $X_O = 1/3$) compared to neutrality, independently defined in both cases (Fig. 6). Only the sub-solidus field is represented in (a) and (b). c. Concentration of C-bearing anions in the fluid (black lines, including CO_3^{2-} , HCO_3^- , $NaCO_3^-$ and $HCOO^-$) at 0.8 GPa (dashed), and 2.5 GPa (continuous), and corresponding fraction of C-bearing anions (in % of total anions, blue lines). It shows a disconnect between the total C content (Fig. 2), abundance and molar fraction of C-bearing anion in a COH fluid at equilibrium with a metapelite. It should be noted that in the presence of carbonates, or of conditions more oxidizing than those prevailing at $X_O = 1/3$, the molar fraction carbon and oxygen [$Y_C = n_C / (n_C + n_O + n_H)$] and $Y_O = n_O / (n_C + n_O + n_H)$] increase in the fluid (e.g., Connolly and Cesare, 1993). This should result in the increase of the abundance of C-bearing anions in the fluid and to larger ΔpH_c values.

uniform along P - T paths 1 and 2. By contrast, pH fluctuations span *ca.* 2 log units along typical high P exhumation paths. Na^+ and OH^- are the predominant charge balancing species in model #1 (Fig. 6). The anionic species $HSiO_3^-$ also contributes at elevated P and low T (upper-left quadrant in Figs. 4–7). This is supported by the observation that the couple $Na^+ - HSiO_3^-$ predominates at blueschist–eclogite facies conditions (Fig. 6a) when $HSiO_3^-$ is added to the calculation. The increased abundance of OH^- at elevated P - T conditions (Fig. 3b) may favor the formation of hydroxo-metal complexes of economic interest, supporting a mechanism previously hypothesized by Hack and Mavrogenes (2006) (*cf.* Seward et al., 2014). A possible role for silica in trace element complexing via formation of $[M^{n+}HSiO_3^-]^{(n-1)+}$ complex at elevated P , *i.e.* blueschist to eclogite facies, may also be proposed, and future experimental works are needed to validate this hypothesis. The effect of isothermal P increase or decrease from the position of Eq. (9) is to bring the fluid closer to neutrality. The temperature dependence of $\Delta pH_{m\#1}$ increases as geothermal gradients

become steeper. Thus, moderate variations $\Delta pH_{m\#1}$ are predicted along the isobaric heating (path #2, Fig. 6d) and the prograde subduction paths. Larger variations are predicted by burial along high P exhumation. These display a U shape pattern inherited from the patterns of $\mathcal{E}_{H^+}^{Na^+}$ and $\mathcal{E}_{H^+}^{K^+}$ (Fig. 5a, b).

The addition of C (model #2) induces important pH differences in the fluid relative to those found in model #1 at the same conditions. Values of pH are lower (Fig. 6a) and systematically closer to neutrality (*i.e.* Fig. 3b) in model #2 than in model #1 at all P and T conditions (Figs. 6d and 7a, b). That is, the relative alkalinity, defined here as $\Delta pH_c = \Delta pH_{m\#1} - \Delta pH_{m\#2}$ with $\Delta pH_{m\#2} = pH_{m\#2} - pH_w^{mix}$ (Figs. 3b, 7a), is everywhere positive and span the range 0.1 to 0.6 (Fig. 7b). Yet, we observe that this effect of C becomes less pronounced (ΔpH_c diminishes) as P and T rise along isolines of C molalities (Fig. 2). These changes can be ascribed to (1) modifications induced to mineral compositions by virtue of Eq. (6), (2) modification of the fluid speciation by the presence of additional C-bearing ions, *e.g.*, HCO_3^- , $HCOO^-$, $NaCO_3^-$,

CaHCO_3^+ and CO_3^{2-} , (3) modification of the solvent properties. The first (mineralogic) and second (speciation) factors are dominant at $T < 600^\circ\text{C}$ where the $\Delta p\text{H}_c$ isolines are tied to the main phase boundaries. However, both effects on the decrease of the fluid alkalinity at low T are dampened, until ca. 600°C , by the progressive decrease of $(\epsilon_r)_{\text{mix}}$ (Fig. 3a), and its effect on the decrease of CO_2 ionization (e.g., Wen and Olesik, 2000). This is reflected in the drop of the molar fraction of C-bearing anions in the fluid (Fig. 7c) to ca. 600°C . With further heating ($T > 600^\circ\text{C}$), the isobaric increase of $\Delta p\text{H}_c$ parallels the increasing fraction of C-bearing anions of intermediate C valence state (predominantly HCOO^- at $T > 600^\circ\text{C}$ and $P < 2$ GPa) in the total anion budget of the fluid (Fig. 7c), simultaneously to the decrease of their concentration and of the ionic strength, and despite the dramatic increase of C solubility (Figs. 1–3). The ionic strength is similar within uncertainty between model #1 and #2 at $P > 1.5$ GPa. However, model #2 returns an ionic strength ca. 4 times higher at low T and low P , and lower by 1–2 orders of magnitude at elevated T and low P than that of model #1. The formation of HCOO^- is favored by the up- T isobaric increase of $f(\text{H}_2)$ at constant X_{O} , a redox-dependent mechanism that would require experimental validation. Overall, these results highlight a direct feedback of redox conditions on acid–base properties of metamorphic fluids. We also find that the bicarbonate ion predominates over other anions in this model at low T and up to ca. 2 GPa, a domain where C molality (ca. 0.02 to 2 molal) and $(\epsilon_r)_{\text{mix}}$ (ca. 15 to 40) are both high enough to favor the presence of ionic C-bearing ligands. Conversely, at $P = 2.5$ GPa and low T , the amount of C bearing anions in the fluid is similar to that at 0.8 GPa (Fig. 7c), increases towards elevated T conditions, but is never predominant in the anionic budget of the fluid. Owing to alkaline pH, the existence of this ionic C pool increases [C] by a factor 2 to 10 ([C] ~ 0.1 molal) at 2–3 GPa and 400–500 $^\circ\text{C}$ (SOM Fig. 4) compared to estimates from a purely molecular model (Connolly and Cesare, 1993, cf. Fig. 2 and SOM Fig. 4).

5. Conclusion

- [1] This work presents a new route to retrieve information on aqueous speciation by bridging conventional chemical petrology with mixed-solvent solution chemistry. It is applicable to a range of rock-dominated high-pressure conditions, including subduction zones. The comparison of predictions from such a model with independent experimental data offers a unique window into elusive processes of ionic association at elevated P and T . Enhancing the accuracy of such predictions requires continued improvement of the consistency between mineral and solute thermochemical data sets (cf. Sverjensky et al., 1991; Holland and Powell, 1998, p. 314; and Appendix B).
- [2] Na-bearing mineral solid-solutions exert the main petrologic control on the acid–base budget of fluids in the models investigated. Thus, our results highlight a decoupling between the abundance of major/minor element in rocks (Na_2O ca. 2 wt% here), and their role on fluid speciation and properties. Predicted pH for both models is alkaline at low P but is closer to neutrality as P increases above the albite–jadeite–quartz transition. It shows little variation along subduction or isobaric heating P – T paths, and large fluctuations of up to 2 log units along model retrograde paths.
- [3] The decrease of $(\epsilon_r)_{\text{mix}}$ in COH fluids dampens H_2O and CO_2 ionization. Combined with the presence of additional C bearing ligands, the overall effect of C is to bring the pH of the system closer to neutrality by up to ca. 0.6 pH at low T and P . C-bearing anions, i.e. HCO_3^- (and HCOO^-), are the dominant ligands at low P despite their limited amount in the fluid. These also represent a non-negligible fraction (up to ca. 50%) of the total anion budget at elevated P and T . Although

few studies have experimentally determined the role of aqueous C on major and trace elements complexation at elevated P and T conditions relevant for subduction zones (Tsai et al., 2014), our work highlights that C-bearing ligands may be available for this purpose. Understanding the full implications of these redox–electrostatic processes on the behavior, budget and recycling of C–N–S volatiles and their isotopes (e.g., Hayes and Waldbauer, 2006), and on ore–metal complexation, transport and deposition (e.g. Phillips and Evans, 2004) to upper mantle P and T , would be a promising target for future investigations.

- [4] The existence of Al–Si and alkali–Al–Si polymer has long been inferred in simple mineral–fluid systems (e.g., Manning et al., 2010). By comparing our results to experimental solubility data, we extend this conclusion to more complex compositional systems, and suggest that metal complex and polymerized species may be more numerous than has previously been appreciated. We show that Ca, Mg, K–Si and K–Al–Si species are required. The extent of these discrepancies, in particular for Ca and Mg, calls for dedicated experimental characterization and/or first-principles MD simulation of the stoichiometric, charge and thermochemical properties of these species. This would be a decisive step toward the accurate quantification of the interactions between compositionally variable lithologies (e.g., Konrad-Schmolke et al., 2011; Galvez et al., 2013b; Marchesi et al., 2013; Angiboust et al., 2014) and complex aqueous solutions associated to deep Earth metasomatism, while preserving a physically realistic model of fluid speciation.
- [5] Future applications of our method to natural systems will require additional considerations: carbonate, sulfate, sulfides, phosphates, borate, multicomponent polymeric anions, and halogen (e.g., Newton and Manning, 2010) can all exert important roles as charge-balancing anions and as ligands. The present study lays the foundation for future works investigating the consequence of these additional sources of complexity on the composition and speciation of metamorphic fluids.

Acknowledgements

We are indebted to Deborah Smith, Allan Harvey, Mark Cad-dick, Paul Asimow and Dimitri Sverjensky for providing valuable insights on various computational or theoretical aspects of this work at an early stage of the project. We thank Lucie Tajcmanova, Chris Glein, Xin Zhong, David Dolejs, Nikolai Akinfiev, George Cody, Peter Ulmer, Jay Ague, Dan Miron and Shuhei Ohara for helpful discussions. The authors wish to acknowledge thorough reviews by John Walther and Bruce Yardley that substantially improved this manuscript, as well as helpful reviews by Simone Tumiat and Isabelle Daniel. We thank B. Marty for editorial guidance and handling. This project was conceived and conducted at the Geophysical Laboratory (CIW) where the first author benefited from a Carnegie Fellowship. A NASA early career collaboration award and an ETH fellowship ETH/CoFUND Fel-06 13-2 (M.E.G.), the US National Science Foundation grant EAR 1347987 (C.E.M.), and support from Deep Carbon Observatory are gratefully acknowledged.

Appendix. Supplementary material

Supplementary material related to this article can be found online at <http://dx.doi.org/10.1016/j.epsl.2015.06.019>.

References

- Ague, J.J., 1994. Mass transfer during Barrovian metamorphism of pelites, south-central Connecticut; I. Evidence for changes in composition and volume. *Am. J. Sci.* 294 (8), 989–1057.

- Ague, J.J., Nicolescu, S., 2014. Carbon dioxide released from subduction zones by fluid-mediated reactions. *Nat. Geosci.* 7 (5), 355–360.
- Angiboust, S., Pettke, T., De Hoog, J.C., Caron, B., Oncken, O., 2014. Channelized fluid flow and eclogite-facies metasomatism along the subduction shear zone. *J. Petrol.* 55 (5), 883–916.
- Aranovich, L.Y., Newton, R.C., 1999. Experimental determination of CO₂–H₂O activity–composition relations at 600–1000 °C and 6–14 kbar by reversed decarbonation and dehydration reactions. *Am. Mineral.* 84, 1319–1332.
- Archer, D.G., Wang, P., 1990. The dielectric constant of water and Debye–Hückel limiting law slopes. *J. Phys. Chem. Ref. Data* 19, 371–411.
- Bandura, A.V., Lvov, S.N., 2006. The ionization constant of water over wide ranges of temperature and density. *J. Phys. Chem. Ref. Data* 35, 15–30.
- Bebout, G.E., Barton, M.D., 1993. Metasomatism during subduction: products and possible paths in the Catalan Schist, California. *Chem. Geol.* 108 (1), 61–92.
- Botti, A., Bruni, F., Mancinelli, R., Ricci, M.A., Lo Celso, F., Triolo, R., Ferrante, F., Soper, A.K., 2008. Study of percolation and clustering in supercritical water–CO₂ mixtures. *J. Chem. Phys.* 128 (16), 164504.
- Bowers, T.S., Jackson, K.J., Helgeson, H.C., 1984. Equilibrium Activity Diagrams: For Coexisting Minerals and Aqueous Solutions at Pressures and Temperatures to 5 kb and 600 °C. Springer, Berlin.
- Bucholz, C.E., Ague, J.J., 2010. Fluid flow and Al transport during quartz-kyanite vein formation, Unst, Shetland Islands, Scotland. *J. Metamorph. Geol.* 28, 19–39.
- Caciagli, N.C., Manning, C.E., 2003. The solubility of calcite in water at 6–16 kbar and 500–800 °C. *Contrib. Mineral. Petrol.* 146, 275–285.
- Caddick, M.J., Thompson, A.B., 2008. Quantifying the tectono-metamorphic evolution of pelitic rocks from a wide range of tectonic settings: mineral compositions in equilibrium. *Contrib. Mineral. Petrol.* 156, 177–195.
- Carswell, D.A., Brueckner, H.K., Cuthbert, S.J., Mehta, K., O'Brien, P.J., 2003. The timing of stabilisation and the exhumation rate for ultra-high pressure rocks in the Western Gneiss Region of Norway. *J. Metamorph. Geol.* 21 (6), 601–612.
- Connolly, J.A.D., Cesare, B., 1993. C–O–H–S fluid composition and oxygen fugacity in graphitic metapelites. *J. Metamorph. Geol.* 11, 379–388.
- Dandurand, J.L., Schott, J., 1992. Prediction of ion association in mixed-crustal fluids. *J. Phys. Chem.* 96, 7770–7777.
- Deul, R., Franck, E., 1991. The static dielectric constant of the water–benzene mixture system to 400 °C and 2800 bar. *Ber. Bunsenges. Phys. Chem.* 95, 847–853.
- Dolejš, D., 2013. Thermodynamics of aqueous species at high temperatures and pressures: equations of state and transport theory. *Rev. Mineral. Geochem.* 76 (1), 35–79.
- Dolejš, D., Manning, C.E., 2010. Thermodynamic model for mineral solubility in aqueous fluids: theory, calibration and application to model fluid–flow systems. *Geofluids* 10 (1–2), 20–40.
- Dubessy, J., Moissette, A., Bakker, R.J., Frantz, J.D., Zhang, Y.G., 1999. High-temperature Raman spectroscopic study of H₂O–CO₂–CH₄ mixtures in synthetic fluid inclusions; first insights on molecular interactions and analytical implications. *Eur. J. Mineral.* 11, 23–32.
- Evans, K.A., Gordon, R.A., Mavrogenes, J.A., Tailby, N., 2009. The effect of CO₂ on the speciation of RbBr in solution at temperatures to 579 °C and pressures to 0.26 GPa. *Geochim. Cosmochim. Acta* 73 (9), 2631–2644.
- Evans, K.A., Phillips, G.N., Powell, R., 2006. Rock-buffering of auriferous fluids in altered rocks associated with the golden mile-style mineralization, Kalgoorlie Gold Field, Western Australia. *Econ. Geol.* 101, 805–817.
- Fernandez, D.P., Goodwin, A.R.H., Lemmon, E.W., Sengers, J.L., Williams, R.C., 1997. A formulation for the static permittivity of water and steam at temperatures from 238 K to 873 K at pressures up to 1200 MPa, including derivatives and Debye–Hückel coefficients. *J. Phys. Chem. Ref. Data* 26 (4), 1125–1166.
- Frezzotti, M.L., Selverstone, J., Sharp, Z.D., Compagnoni, R., 2011. Carbonate dissolution during subduction revealed by diamond-bearing rocks from the Alps. *Nat. Geosci.* 4 (10), 703–706.
- Fyfe, W.S., Price, N.J., Thompson, A.B., 1978. Fluids in the Earth's Crust. Elsevier, Amsterdam.
- Galvez, M.E., Beyssac, O., Martinez, I., Benzerara, K., Chaduteau, C., Malvoisin, B., Malavieille, J., 2013a. Graphite formation by carbonate reduction during subduction. *Nat. Geosci.* 6, 473–477.
- Galvez, M.E., Martinez, I., Beyssac, O., Benzerara, K., Agrinier, P., Assayag, N., 2013b. Metasomatism and graphite formation at a lithological interface in Malaspina (Alpine Corsica, France). *Contrib. Mineral. Petrol.* 166, 1687–1708.
- Hack, A.C., Mavrogenes, J.A., 2006. A synthetic fluid inclusion study of copper solubility in hydrothermal brines from 525 to 725 °C and 0.3 to 1.7 GPa. *Geochim. Cosmochim. Acta* 70, 3970–3985.
- Harvey, A.H., Lemmon, E.W., 2005. Method for estimating the dielectric constant of natural gas mixtures. *Int. J. Thermophys.* 26, 31–46.
- Harvey, A.H., Prausnitz, J.M., 1987. Dielectric constants of fluid mixtures over a wide range of temperature and density. *J. Solution Chem.* 16, 857–869.
- Hayes, J.M., Waldbauer, J.R., 2006. The carbon cycle and associated redox processes through time. *Philos. Trans. R. Soc. B. Biol. Sci.* 361 (1470), 931–950.
- Helgeson, H.C., 1968. Evaluation of irreversible reactions in geochemical processes involving minerals and aqueous solutions – I. Thermodynamic relations. *Geochim. Cosmochim. Acta* 32, 853–877.
- Helgeson, H.C., Kirkham, D.H., 1976. Theoretical prediction of the thermodynamic properties of aqueous electrolytes at high pressures and temperatures. III. Equation of state for aqueous species at infinite dilution. *Am. J. Sci.* 276, 97–240.
- Helgeson, H.C., Kirkham, D.H., Flowers, G.C., 1981. Theoretical prediction of the thermodynamic behavior of aqueous electrolytes by high pressures and temperatures. IV. Calculation of activity coefficients, osmotic coefficients, and apparent molal and standard and relative partial molal properties to 600 °C and 5 kb. *Am. J. Sci.* 281, 1249–1516.
- Holland, T., Powell, R., 1991. A Compensated-Redlich–Kwong (CORK) equation for volumes and fugacities of CO₂ and H₂O in the range 1 bar to 50 kbar and 100–1600 °C. *Contrib. Mineral. Petrol.* 109, 265–273.
- Holland, T., Powell, R., 2003. Activity-composition relations for phases in petrological calculations: an asymmetric multicomponent formulation. *Contrib. Mineral. Petrol.* 145, 492–501.
- Holland, T.J.B., Powell, R., 1998. An internally consistent thermodynamic data set for phases of petrological interest. *J. Metamorph. Geol.* 16, 309–343.
- Kirkwood, J.G., 1939. The dielectric polarization of polar liquids. *J. Chem. Phys.* 7, 911–919.
- Konrad-Schmolke, M., Zack, T., O'Brien, P.J., Barth, M., 2011. Fluid migration above a subducted slab—Thermodynamic and trace element modelling of fluid–rock interaction in partially overprinted eclogite-facies rocks (Sesia Zone, Western Alps). *Earth Planet. Sci. Lett.* 311 (3), 287–298.
- Landau, L.D., Lifshitz, M., 1960. *Electrodynamics of Continuous Media*. Pergamon Press, Oxford.
- Looyenga, H., 1965. Dielectric constants of heterogeneous mixtures. *Physica* 31, 401–406.
- Malvoisin, B., Chopin, C., Brunet, F., Galvez, M.E., 2012. Low-temperature wollastonite formed by carbonate reduction: a marker of serpentinite redox conditions. *J. Petrol.* 53 (1), 159–176.
- Manning, C.E., 1994. The solubility of quartz in H₂O in the lower crust and upper mantle. *Geochim. Cosmochim. Acta* 58, 4831–4839.
- Manning, C.E., 1998. Fluid composition at the blueschist–eclogite transition in the model system Na₂O–MgO–Al₂O₃–SiO₂–H₂O–HCl. *Schweiz. Mineral. Petrogr. Mitt.* 78, 225–242.
- Manning, C.E., Antignano, A., Lin, H.A., 2010. Premelting polymerization of crustal and mantle fluids, as indicated by the solubility of albite + paragonite + quartz in H₂O at 1 GPa and 350–620 °C. *Earth Planet. Sci. Lett.* 292, 325–336.
- Marchesi, C., Garrido, C.J., Padrón-Navarta, J.A., Sánchez-Vizcaíno, V.L., Gómez-Pugnaire, M.T., 2013. Element mobility from seafloor serpentinitization to high-pressure dehydration of antigorite in subducted serpentinite: insights from the Cerro del Almiraz ultramafic massif (southern Spain). *Lithos* 178, 128–142.
- Marshall, W.L., Franck, E.U., 1981. Ion product of water substance, 0–1000 °C, 1–10,000 bars new international formulation and its background. *J. Phys. Chem. Ref. Data* 10, 295–304.
- Mysen, B.O., 2010. Speciation and mixing behavior of silica-saturated aqueous fluid at high temperature and pressure. *Am. Mineral.* 95, 1807–1816.
- Newton, R.C., Manning, C.E., 2010. Role of saline fluids in deep-crustal and upper-mantle metasomatism: insights from experimental studies. *Geofluids* 10, 58–72.
- Pak, T.M., Hauenberger, C.A., Baumgartner, L.P., 2003. Solubility of the assemblage albite + K-feldspar + andalusite + quartz in supercritical aqueous chloride solutions at 650 °C and 2 kbar. *Chem. Geol.* 200, 377–393.
- Pan, D., Spanu, L., Harrison, B., Sverjensky, D.A., Galli, G., 2013. Dielectric properties of water under extreme conditions and transport of carbonates in the deep Earth. *Proc. Natl. Acad. Sci. USA* 110, 6646–6650.
- Penniston-Dorland, S.C., Ferry, J.M., 2008. Element mobility and scale of mass transport in the formation of quartz veins during regional metamorphism of the Waits River Formation, east-central Vermont. *Am. Mineral.* 93 (1), 7–21.
- Phillips, G.N., Evans, K.A., 2004. Role of CO₂ in the formation of gold deposits. *Nature* 429 (6994), 860–863.
- Pokrovskii, V.A., Helgeson, H.C., 1997. Thermodynamic properties of aqueous species and the solubilities of minerals at high pressures and temperatures: the system Al₂O₃–H₂O–KOH. *Chem. Geol.* 137, 221–242.
- Schmidt, C., 2014. Raman spectroscopic determination of carbon speciation and quartz solubility in H₂O + Na₂CO₃ and H₂O + NaHCO₃ fluids to 600 °C and 1.53 GPa. *Geochim. Cosmochim. Acta* 145, 281–296.
- Seward, T.M., Williams-Jones, A.E., Migdisov, A.A., 2014. The chemistry of metal transport and deposition by ore forming hydrothermal fluids. In: *Treatise on Geochemistry*, vol. 13, 2nd edition. Elsevier, Amsterdam, pp. 29–57.
- Shock, E.L., Oelkers, E.H., Johnson, J.W., Sverjensky, D.A., Helgeson, H.C., 1992. Calculation of the thermodynamic properties of aqueous species at high pressures and temperatures. Effective electrostatic radii, dissociation constants and standard partial molal properties to 1000 °C and 5 kbar. *J. Chem. Soc., Faraday Trans.* 88, 803–826.
- Spandler, C., Mavrogenes, J., Hermann, J., 2007. Experimental constraints on element mobility from subducted sediments using high-P synthetic fluid/melt inclusions. *Chem. Geol.* 239, 228–249.
- Sverjensky, D.A., Harrison, B., Azzolini, D., 2014. Water in the deep Earth: the dielectric constant and the solubilities of quartz and corundum to 60 kb and 1200 °C. *Geochim. Cosmochim. Acta* 129, 125–145.

- Sverjensky, D.A., Hemley, J., d'Angelo, W., 1991. Thermodynamic assessment of hydrothermal alkali feldspar-mica-aluminosilicate equilibria. *Geochim. Cosmochim. Acta* 55, 989–1004.
- Sverjensky, D.A., Shock, E.L., Helgeson, H.C., 1997. Prediction of the thermodynamic properties of aqueous metal complexes to 1000 °C and 5 kb. *Geochim. Cosmochim. Acta* 61, 1359–1412.
- Syracuse, E.M., van Keken, P.E., Abers, G.A., 2010. The global range of subduction zone thermal models. *Phys. Earth Planet. Inter.* 183, 73–90.
- Tanger, J.C., Helgeson, H.C., 1988. Calculation of the thermodynamic and transport properties of aqueous species at high pressures and temperatures; revised equations of state for the standard partial molal properties of ions and electrolytes. *Am. J. Sci.*, 19–98.
- Tropper, P., Manning, C., 2007. The solubility of corundum in H₂O at high pressure and temperature and its implications for Al mobility in the deep crust and upper mantle. *Chem. Geol.* 240, 54–60.
- Tsay, A., Zajacz, Z., Sanchez-Valle, C., 2014. Efficient mobilization and fractionation of rare-earth elements by aqueous fluids upon slab dehydration. *Earth Planet. Sci. Lett.* 398, 101–112.
- Wang, P., Anderko, A., 2001. Computation of dielectric constants of solvent mixtures and electrolyte solutions. *Fluid Phase Equilib.* 186 (1), 103–122.
- Walther, J.V., 1992. Ionic association in H₂O–CO₂ fluids at mid-crustal conditions. *J. Metamorph. Geol.* 10, 789–797.
- Walther, J.V., Helgeson, H.C., 1980. Description and interpretation of metasomatic phase relations at high pressures and temperatures. 1. Equilibrium activities of ionic species in nonideal mixtures of CO₂ and H₂O. *Am. J. Sci.* 280, 575–606.
- Walther, J.V., Schott, J., 1988. The dielectric constant approach to speciation and ion pairing at high temperature and pressure. *Nature*, 635–638.
- Wen, D., Olesik, S.V., 2000. Characterization of pH in liquid mixtures of methanol/H₂O/CO₂. *Anal. Chem.* 72, 475–480.
- Widmer, T., Thompson, A.B., 2001. Local origin of high pressure vein material in eclogite facies rocks of the Zermatt-Saas Zone, Switzerland. *Am. J. Sci.* 301 (7), 627–656.
- Wohlers, A., Manning, C.E., 2009. Solubility of corundum in aqueous KOH solutions at 700 °C and 1 GPa. *Chem. Geol.* 262, 310–317.
- Wohlers, A., Manning, C.E., Thompson, A.B., 2011. Experimental investigation of the solubility of albite and jadeite in H₂O, with paragonite + quartz at 500 and 600 °C, and 1–2.25 GPa. *Geochim. Cosmochim. Acta* 75, 2924–2939.
- Wolery, T.J., 1992. EQ3/6: A software package for geochemical modeling of aqueous systems: package overview and installation guide (version 7.0). Lawrence Livermore National Laboratory, Livermore, CA.
- Yardley, B.W.D., Graham, J.T., 2002. The origins of salinity in metamorphic fluids. *Geofluids* 2, 249–256.
- Yoshii, N., Miura, S., Okazaki, S., 2001. A molecular dynamics study of dielectric constant of water from ambient to sub- and supercritical conditions using a fluctuating-charge potential model. *Chem. Phys. Lett.* 345 (1), 195–200.
- Zhang, Z., Duan, Z., 2005. Prediction of the PVT properties of water over wide range of temperatures and pressures from molecular dynamics simulation. *Phys. Earth Planet. Inter.* 149, 335–354.
- Zotov, N., Keppler, H., 2000. In-situ Raman spectra of dissolved silica species in aqueous fluids to 900 °C and 14 kbar. *Am. Mineral.* 85, 600–604.

The solubility of rocks in metamorphic fluids: A model for rock-dominated conditions to upper mantle pressure and temperature

APPENDICES – Galvez et al. EPSL 2015

A. POLARIZATION, RELATIVE PERMITTIVITY, VOLUME FRACTION AND DENSITY OF NON-POLAR AND POLAR COMPONENTS.

Polarization and relative permittivity

Here we briefly describe the Debye–Onsager–Kirkwood model, refined by Harvey and Prausnitz (1987) for mixtures (“DOK–HP” model), and adapted here to model the solvent properties of C-saturated COH fluids ($X_{\text{O}}=1/3$) and to include updated values for $(\epsilon_r)_{\text{H}_2\text{O}}$ to upper mantle P and T (Pan et al., 2013; Sverjensky et al., 2014).

The Kirkwood equation for polar liquids (Kirkwood, 1939),

$$\mathcal{P} = (2\epsilon_r + 1)(\epsilon_r - 1)/9\epsilon_r \quad (1),$$

is used to derive the polarization per unit volume (\mathcal{P}) of H_2O from its relative permittivity $(\epsilon_r)_{\text{H}_2\text{O}}$, which is computed with an EoS from Sverjensky et al. (2014) with input H_2O densities from Zhang and Duan (2005). Eq. (1) is also used to compute the relative permittivity of the polar COH mixture from its polarization (\mathcal{P}_{mix}). The polarization is classically described as the sum of two contributions (e.g., Onsager, 1936; Kirkwood, 1939):

(1) The *induced polarization* of the molecules. It comprises the electronic and atomic polarization. In Kirkwood’s theory (1939), the former is proportional to the electronic polarizability α , and the latter is neglected.

(2) The *orientation polarization* of the dipoles which is a function of the permanent dipole moment of the molecules and of their orientational ordering, represented by the Kirkwood correlation factor (g_K).

The polarization of individual non-polar molecular species of the mixture (CO_2 and CH_4) is computed, at T and P , using an empirical formulation of \mathcal{P}/ρ_m expressed as a power series in the molar density, i.e. $(\rho_m)_i = 1/v_i$, ($\text{mol}\cdot\text{cm}^{-3}$), where the coefficients have been made slightly T dependent (Harvey and Lemmon, 2005). The first coefficient of this expansion is proportional to α , i.e. to the induced polarization of the non-polar molecules. These values of \mathcal{P} are used to derive the relative permittivity of CO_2 and CH_4 with the Clausius–Mosotti relation:

$$\mathcal{P} = (\epsilon_r - 1)/(\epsilon_r + 2) \quad (2)$$

Because Eq. (1) is used to derive $(\epsilon_r)_{\text{mix}}$ from \mathcal{P}_{mix} (Harvey and Prausnitz, 1987), consistency requires equivalent values of \mathcal{P} for each of the non-polar components to be computed from their relative permittivity using Eq. (1). \mathcal{P}_{mix} is then computed by linear combination (e.g., Debye, 1929; Kirkwood, 1939) with,

$$\mathcal{P}_{\text{mix}} = \sum_i V_{f,i} \mathcal{P}_i \quad (3)$$

where $V_{f,i}$ is the volume fraction of species i in the COH mixture at P and T . Consequently, Eq. (3) implicitly assumes that the orientation polarization of H_2O dipoles (i.e. g_K -factor) is unchanged upon mixing. This assumption is likely to be invalid in the general case (e.g., Deul and Franck, 1991; Dubessy et al., 1999; Botti et al., 2008), but the discrepancies introduced by this assumption have a negligible effect on the conclusions of this study.

Volume fractions and density

In Eq. (3), $V_{f,i}$ at P and T is computed using a method developed by Harvey and Prausnitz (1987),

$$V_{f,i} = \frac{x_i v_i^*}{\sum_j x_j v_j^*} \quad (4)$$

where x_i and v_i^* are the molar fraction of species i at P and T , and the reference molar volume of species i at critical conditions, respectively. The values of v_i^* used are $94.119 \text{ cm}^3\cdot\text{mol}^{-1}$ (CO_2), $98.629 \text{ cm}^3\cdot\text{mol}^{-1}$ (CH_4). CO and H_2 were neglected in the computation of $(\epsilon_r)_{\text{mix}}$ due to their low predicted abundance, $X(\text{CO}) < X(\text{H}_2) < 0.01$, at all conditions of this study. The values of $(\rho_m)_i$ in the mixture, used in Eq. (1) and (2), are computed by scaling back molar densities at critical conditions (i.e., $1/v_i^*$) to P and T of interest (Harvey and Prausnitz,

1987). This is accomplished by using the reduced density κ as the scaling factor, and defined as:

$$\kappa(P, T) = \frac{(\rho_m)_{\text{mix}}(P, T)}{(\rho_m)_{\text{mix}}^*} \quad (5)$$

where $(\rho_m)_{\text{mix}}$ and $(\rho_m)_{\text{mix}}^*$ are the molar density of the mixture at P and T (Connolly and Cesare, 1993) and at critical conditions [$(\rho_m)_{\text{mix}}^* = 1/\sum_i x_i v_i^*$], respectively. Using Eq. (4) and (5) yields,

$$(\rho_m)_i(P, T) = \frac{\kappa(P, T)}{v_i^*} \quad (6)$$

This scheme has the advantage of explicitly accounting for the excess volume of mixing in the solution via Eq. (5) and the EoS of Connolly and Cesare (1993), compared to other mixing rules such as that of Oster (1946).

For comparison, values of $(\rho_m)_i$ have also been retrieved from the partial molar volumes of each species using,

$$(\rho_m)_i = \frac{1}{RT} \frac{\partial P}{\partial \ln f_i} \quad (7)$$

where f_i is the fugacity of species i in the mixture. The results obtained for $(\epsilon_r)_{\text{mix}}$ with this alternate scheme are similar within uncertainties to those obtained with the original method based on Eq. (6).

Alternatively, and contrary to the DOK–HP model applying Eq. (3), the Landau–Lifshitz–Looyenga (LLL model) mixing model (Landau and Lifshitz, 1960, Sec. II, 9; Looyenga, 1965) makes the approximation that the cube root of ϵ_r is additive (cf. Walther and Schott, 1988; Walther, 1992, for applications):

$$(\epsilon_r)_{\text{mix}}^{1/3} = \sum_i V_{f,i} (\epsilon_r)_i^{1/3} \quad (8)$$

Using this approach, combined with $V_{f,i}$ calculated with Eq. (4) to account for excess volume of mixing (Harvey and Prausnitz, 1987; Connolly and Cesare, 1993), returns $(\epsilon_r)_{\text{mix}}$ values that are typically lower by ca. 2 to 5 % (max 12 %) at subsolidus conditions than those retrieved with our adaptation of the DOK–HP mixing model. The discrepancies peak at 16% at $T > 700 \text{ }^\circ\text{C}$ and $P = 0.4 - 0.5 \text{ GPa}$. These results are predictable by injecting Eq. (2) in Eq. (1) (DOK–HP model), and by injecting Eq. (1) in Eq. (3) (LLL model) and comparing both expressions (i.e. $(\epsilon_r)_{\text{mix}}$) as functions of $V_{f,i}$ and \mathcal{P}_i . It can be shown, for a binary polar-nonpolar system, that $(\epsilon_r)_{\text{DOK-HP}} - (\epsilon_r)_{\text{LLL}}$ and the ratio $(\epsilon_r)_{\text{DOK-HP}} - (\epsilon_r)_{\text{LLL}} / (\epsilon_r)_{\text{LLL}}$ are positive, present a maximum for $V_{f,2} = 0.45$ and $V_{f,2} = 0.6$ to 0.8 respectively ($V_{f,2}$ is the volume fraction of the nonpolar species), and that their values are positively correlated with the disparities in polarization of intermixing species.

A previous study have shown that the LLL model reproduces experimental measurements of the dielectric properties of polar-nonpolar (i.e. water-benzene) mixtures to supercritical conditions (i.e. to $400 \text{ }^\circ\text{C}$ and 0.28 GPa) with great accuracy, i.e. typically within 1–5% (Deul and Franck, 1991), but the authors did not compare its performance to the DOK–HP mixing model. Further works at geologic conditions are needed to test the relative performance of both frameworks in computing $(\epsilon_r)_{\text{mix}}$ of polar-non-polar solvent mixtures (Mountain and Harvey, in preparation).

The results of our study are unaffected by the use of one or the other alternatives given the low amount of C dissolved in the fluid at subsolidus conditions, and given the weakly polar nature of H_2O (i.e. low $\mathcal{P}_{\text{H}_2\text{O}}$) at elevated T and low P despite higher C solubility. However, for fluid-rock systems characterized by elevated C concentrations, such as those affected by prograde decarbonation in subduction (Connolly and Cesare, 1993; Galvez et al. in preparation), in polar aqueous mixtures (high P), the demonstrated performance of the LLL mixing approach (Deul and Franck, 1991) combined with $V_{f,i}$ computed from Harvey and Prausnitz (1987) should be provisionally preferred.

B. CONVENTIONS AND COMPUTATIONAL DETAILS

Conventions and thermochemical databases

The EoS for the graphite-saturated COH fluid is from Connolly and Cesare (1993) which computes fugacities of H_2O and CO_2 from Holland and Powell (1991, 1998), CH_4 from Jacobs and Kerrick (1981), and H_2 and CO from Redlich and Kwong (1949). Activity coefficients are computed by combining each individual species fugacity with a modified Redlich–Kwong mixing rule modified by Connolly and Cesare (1993) from de Santis et al. (1974) and Holloway (1977) [cf method by Connolly (1995)]. Thermochemical properties for minerals are from the 2002 revision (HP02ver.dat) of the Holland and

Powell database (1998), and those of aqueous species are from (Shock and Helgeson, 1988; Shock et al., 1997; Sverjensky et al., 1997) as compiled, revised and augmented by Sverjensky et al. (2014).

The apparent Gibbs free energy of formation of a mineral at P and T computed with `Perple_X` (Connolly, 1990), *i.e.* used here to retrieve the chemical potential of oxides (see Eq. (3),(4) in text), and with `Supcrt92/EQ3` (Johnson et al., 1992; Wolery, 1992) using the Berman (1988) database partially revised by Sverjensky et al. (1991), *i.e.* used to regress the standard partial molal Gibbs free energies of a range of aqueous species (*e.g.* $\text{SiO}_{2,\text{aq}}$, $\text{CaCO}_{3,\text{aq}}$, Ca^{2+} and AlO_2^- ; see Facq et al., 2014; Sverjensky et al., 2014), follow the so-called ‘‘Benson–Helgeson’’ convention. Thus, the apparent Gibbs free energy of formation of a mineral is computed as the difference between the absolute Gibbs free energy of the mineral at P and T and the absolute Gibbs free energy of its constituent elements at T_r and P_r (*e.g.*, Benson, 1968; Helgeson et al., 1978; Helgeson et al., 1981; Anderson and Crerar, 1993; Dolejš, 2013). Consequently, the mineral properties (and chemical potential of oxides) used in this work are thermodynamically consistent with the conventions used for the empirical derivation of aqueous species properties. Minor discrepancies in the standard state properties of most endmember minerals between Berman (1988) and Holland and Powell database (1998, 2002 revision), and in the isobaric heat capacity and volumetric functions implemented in `PerpleX` and `SUPCRT92` result in differences in the apparent Gibbs energy of formation of minerals at high P and T within $\pm 1 \text{ kJ}\cdot\text{mol}^{-1}$ for all minerals, *e.g.* Qtz, Cc, Cor, used for the calibration of aqueous species properties. This is sufficiently small that these differences do not materially impact the results reported.

Moreover, while the relative properties of alkali-silicates are well constrained from phase equilibria (Berman, 1988; Berman and Aranovich, 1996; Holland and Powell, 1998; Holland and Powell, 2011), there have been some debate over the accuracy of their absolute properties due to the absence of calorimetric data for pure Na_2O and K_2O . Sverjensky et al. (1991) suggested that a correction of *ca.* -6.7 and $-6.8 \text{ kJ}\cdot\text{mol}^{-1}$ to the enthalpy of formation of K and Na silicates at T_r and P_r in Berman’s database (1988), while leaving their third law entropy and volumes unchanged and with appropriate adjustment of dissociation constants for HCl, would reproduce solubility data of assemblages involving muscovite, quartz, pyrophyllite, K-feldspar, andalusite and kaolinite in HCl solutions from $300 \text{ }^\circ\text{C}$ to $600 \text{ }^\circ\text{C}$ and 1 kbar, and bring into full consistency the properties of most electrolytes with those of minerals.

Independently, translations of similar magnitude have been applied to the enthalpies of Na and K minerals in the updated Berman and Aranovich (1996) and Holland and Powell (1998, 2002 revision) databases, *e.g.* for muscovite ($-7 \text{ kJ}\cdot\text{mol}^{-1}$), sanidine ($-5.5 \text{ kJ}\cdot\text{mol}^{-1}$), microcline ($-4.8 \text{ kJ}\cdot\text{mol}^{-1}$) and albite ($-8.5 \text{ kJ}\cdot\text{mol}^{-1}$). These changes guarantee good consistency between the properties of most Na and K minerals ($\pm 3 \text{ kJ}\cdot\text{mol}^{-1}$ for the Gibbs free energy of jadeite and muscovite at 1 GPa and $600 \text{ }^\circ\text{C}$) derived from the Berman (1988) database revised according to Sverjensky et al. (1991) and the Holland and Powell (1998, 2002 revision) database used here. These modifications also partly explain the very good fit of mineral solubility data (K-bearing assemblage above) reported by Holland and Powell (1998, p. 314) at all temperatures. Yet, a discrepancy of *ca.* $14 \text{ J}\cdot\text{mol}^{-1}\cdot\text{K}^{-1}$ for the third law entropy of albite (Holland and Powell, 1998) compared to the values reported in the Berman’s database (1988) propagates a T -dependent discrepancy for the Gibbs free energy albite, between these two alternative frameworks, reaching *ca.* $10 \text{ kJ}\cdot\text{mol}^{-1}$ at 1 GPa and $600 \text{ }^\circ\text{C}$. Resolving this issue may require the incorporation of high precision Na-K mineral solubility data (in addition to phase equilibria) as part of the least-square optimization of mineral properties in Holland and Powell (1998, p314), as originally done by Berman et al. (1985), and as advocated by Sverjensky et al. (1991). While this may be considered for future prolongations of this work, this is considered outside the scope of the present study. The reader is referred to the interesting discussion on this issue by Berman (1988, p. 454–455), Sverjensky et al. (1991) and Holland and Powell (1998, p. 314). In any case, our estimates show that the internal uncertainties attached to the properties of minerals, *e.g.* $4\text{--}6 \text{ kJ}\cdot\text{mol}^{-1}$ on the enthalpies of Na and K-silicates in Holland and Powell (1998), result in negligible difference in predicted pH (<0.1 unit), and uncertainties around ± 0.1 log unit on the values of $\log[\text{Na}]$, $\log[\text{K}]$ and $\log[\text{Al}]$, and less than 0.1 log unit for $\log[\text{Si}]$.

It should be stressed again that the Holland and Powell databases (1998; 2011) include data for a limited number of aqueous ions which properties were not part of the least-square regression (see Holland and Powell (1998, p314) for details),

to be used with a density model (Holland and Powell, 1998) modified from Anderson et al. (1991). Such an approach may be interesting to pursue as well with the above considerations.

Solvent properties

Here the solvent is considered as a dielectric continuum (*e.g.*, Helgeson et al., 1981; Ehrenson, 1987; Dandurand and Schott, 1992, for details on the model, and alternatives), *i.e.* the values of (ϵ_r) of the bulk solvent are used in the original Born equation (see Eq. (1) in text) and the effects of reduced orientational polarizability and compaction of water dipoles around electrolytes (*i.e.* dielectric saturation) are implicitly taken into account by adjustment of the effective ionic radius which appears in the definition of the conventional Born coefficient $\bar{\omega}$ (*e.g.*, Helgeson and Kirkham, 1976; Helgeson et al., 1981; Shock et al., 1992). At $P < 0.5$ GPa, the conventional Born coefficient $\bar{\omega}$ of solutes is a function of solvent density and T where it is computed using a correlation function from Shock et al. (1992) (Here, the use of another EoS from the original one (Haar, 1984) for H_2O results in negligible differences in $\bar{\omega}$ compared to values reported in (Shock et al., 1992) at similar P and T) and is constant at P exceeding $P = 0.5$ GPa (Tanger and Helgeson, 1988; Shock et al., 1992).

Aqueous species and systems of equation

Model #1 involves 19 unknowns. 12 of which are iteratively solved for electrolyte molalities (*i.e.*, cations Na^+ , K^+ , Ca^{2+} , Mg^{2+} , CaOH^+ , MgOH^+ , H^+ and anions AlO_2^- , OH^- , 10 unknowns), activity coefficients (2 unknowns) and the ionic strength of the system. The remaining 7 are neutral complex molalities (*i.e.* $\text{SiO}_{2,\text{aq}}$, $\text{Si}_2\text{O}_{4,\text{aq}}$, $\text{NaOH}_{,\text{aq}}$, $\text{NaHSiO}_{3,\text{aq}}$, $\text{NaAlO}_{2,\text{aq}}$, $\text{KOH}_{,\text{aq}}$, $\text{HAlO}_{2,\text{aq}}$) directly retrieved from the chemical potential of their corresponding oxides and H_2O , and \bar{g}_j° (Eq. (2),(3) in text).

Model #2 involves 26 unknowns. 17 of which are iteratively solved for electrolyte molalities (*i.e.*, cations Na^+ , K^+ , Ca^{2+} , Mg^{2+} , CaOH^+ , CaHCO_3^+ , MgOH^+ , H^+ , and anions AlO_2^- , OH^- , HCO_3^- , HCOO^- , NaCO_3^- and CO_3^{2-} , 15 unknowns), activity coefficients (2 unknowns) and the ionic strength of the system. The remaining 9 are neutral complex molalities (*i.e.* $\text{SiO}_{2,\text{aq}}$, $\text{Si}_2\text{O}_{4,\text{aq}}$, $\text{NaOH}_{,\text{aq}}$, $\text{NaHSiO}_{3,\text{aq}}$, $\text{NaAlO}_{2,\text{aq}}$, $\text{KOH}_{,\text{aq}}$, $\text{HAlO}_{2,\text{aq}}$, $\text{NaHCO}_{3,\text{aq}}$, $\text{CaCO}_{3,\text{aq}}$) directly retrieved from the chemical potential of their corresponding oxides and H_2O , and \bar{g}_j° (Eq. (2),(3) in text).

Non-ideal activity in the fluid

Non-ideality (excess Gibbs free energy of mixing) in the fluid phase is split into contributions affecting the solvent molecules and the solutes, respectively: the first contribution ($\gamma_{MRK,i}$) affects the solvent species H_2O , CO_2 , CH_4 , H_2 and CO (model #2) as they are mixed with a non-ideal molecular model, *i.e.* (Connolly and Cesare, 1993). The second contribution is electrostatic and represents long-range ionic interactions ($\gamma_{D,j}$).

Long-range ionic interactions in the solution are described by an extended form of the Debye–Huckel expression after Davies (1962), linking the ionic strength of the solution (I) to the activity coefficient $\gamma_{D,j}$ of solute j :

$$\log \gamma_{D,j} = \frac{-AZ_j^2 I^{1/2}}{(1 + I^{1/2})} + 0.2AZ_j^2 I \quad (9)$$

where $I = \frac{1}{2} \sum_j Z_j^2 m_j$, $A = 1.82483 \cdot 10^6 \rho_{\text{mix}}^{1/2} [(\epsilon_r)_{\text{mix}} T]^{-3/2}$ and m_j refers to the molality ($\text{mol}\cdot\text{kg}^{-1} \text{H}_2\text{O}$) of the ion considered, $\gamma_{D,j}$ is considered identical for all monovalent species ($\gamma_{D,1}$) and divalent species ($\gamma_{D,2}$), Z_j is the charge of the electrolyte, A is the Debye-Huckel parameter (*e.g.*, Helgeson and Kirkham, 1974) which provisions for change in solvent density ρ_{mix} (in $\text{g}\cdot\text{cm}^{-3}$) and relative permittivity $(\epsilon_r)_{\text{mix}}$ between the two models, and $\gamma_{D,j} m_j = a_j$. As noted by Manning (2013), results of speciation calculations do not depend significantly on choice of activity model for ionic strengths (I) below 1, which is the case here. For all neutral species, $\gamma_{D,j} = 1$.

Finally, the energetics of ions in going from a pure H_2O fluid to a COH mixture characterized by $(\epsilon_r)_{\text{mix}}$ is incorporated to the standard state Gibbs free energy of the ions in the mixed-solvent (*e.g.*, Walther, 1992; Akinfiev and Zotov, 1999; Pérez-Salado Kamps, 2005), and thus to the equilibrium constants of homogeneous equilibria in the solution. For example, in model #2, the dielectric correction applied to K_w (Bandura and Lvov, 2006) leads to K_w^{mix} according to:

$$\log K_w^{mix} - \log K_w = -\frac{\bar{\omega}_{OH^-}}{2.203RT} \cdot \left(\frac{1}{(\epsilon_r)_{mix}} - \frac{1}{(\epsilon_r)_{H_2O}} \right) \quad (10)$$

In this case, the dielectric correction factor $\theta = \frac{1}{2.203RT} \cdot \left(\frac{1}{(\epsilon_r)_{mix}} - \frac{1}{(\epsilon_r)_{H_2O}} \right)$ ranges from $\theta = 6 \cdot 10^{-8} \text{ mol}\cdot\text{cal}^{-1}$ (400 °C and 3 GPa) to $\theta = 4 \cdot 10^{-5} \text{ mol}\cdot\text{cal}^{-1}$ at the highest C content of the COH mixture (900 °C and 0.2 GPa). Thus θ is everywhere well within the domain of applicability of such corrections in the sub-solidus region, *i.e.* $\theta \ll 3 \cdot 10^{-5} \text{ mol}\cdot\text{cal}^{-1}$ (Akinfiev and Zotov, 1999). Consequently, neutral pH in the molecular mixture, *i.e.* pH_w^{mix} corresponding to $a(H^+) = a(OH^-)$, is given by:

$$pH_w^{mix} = \frac{1}{2} \left(pK_w + \frac{\bar{\omega}_{OH^-}}{2.203RT} \cdot \left(\frac{1}{(\epsilon_r)_{mix}} - \frac{1}{(\epsilon_r)_{H_2O}} \right) - \log(aH_2O) \right) \quad (11)$$

pK_w^{mix}

Equivalent approaches, which maintain the standard state of electrolytes in mixed-solvents referenced to pure H₂O, consider this dielectric correction as part of the excess Gibbs free energy of the system [$\gamma_{solv,j}$ in, *e.g.*, Dandurand and Schott (1992)]. Under this convention, $pK_w^{mix} = pK_w$. The fluid alkalinity, defined as the difference between the pH of the fluid and neutral pH (see also Fig. 6 in text) is insensitive to the choice between these two alternatives.

C. MINERAL SOLUTION MODELS USED

SOLUTION MODELS	Model formula	source
Biotite (Bio)	$K[Mg_xFe_yMn_{1-x-y}]_{3-4-u-v-w}Fe^{3+}_wTi_uAl_{1+v}Si_{3-u}O_{10}(OH)_{2-2u}x+y \leq 1, u+v+w \leq 1$	(Tajcmanova et al., 2009)
Garnet (Gar)	$Fe_3Ca_3Mg_3Mn_3(1-x-y-z)Al_2Si_3O_{12}, x+y+z \leq 1$	(Holland and Powell, 1998)
Chlorite (Chl)	$[Mg_xFe_yMn_{1-x-y}]_{5-y+z}Al_{2(1+y-z)}Si_{3-y+z}O_{10}(OH)_8, x+w \leq 1$	(Holland et al., 1998)
Staurolite (Sta)	$Mg_{4x}Fe_{4y}Mn_{4(1-x-y)}Al_{18}Si_{7.5}O_{48}H_4, x+y \leq 1$	(Mahar et al., 1997)
White mica (Mus, Phe or Par)	$K_yCa_xNa_{1-x-y}(Mg_{1-y}Fe_y)_2Mg_wTi_wAl_{3+x-w}Si_{3-x-z}O_{10}(OH)_2, x+y \leq 1, w+z \leq y$ (here $w=0$)	(Coggon and Holland, 2002), (Auzanneau et al., 2010)
K-feldspars (Kfs)	$Na_xK_{1-x}AlSi_3O_8$	(Waldbaum and Thompson, 1968)
Omphacite (Omp)	$Na_y[CaMg_xFe_{1-x}]_yAl_2Si_2O_6$	(Holland and Powell, 1996)
Cordierite (Crd)	$Mg_{2-x}Fe_xMn_{2(1-x-y)}Al_4Si_5O_{18}*(H_2O)_2, x+y \leq 1$	(Mahar et al., 1997)
Chloritoid (Ctd)	$Mg_xFe_yMn_{1-x-y}Al_2Si_3(OH)_2, x+y \leq 1$	(White et al., 2000)
Orthopyroxene (Opx)	$[Mg_xFe_{1-x}]_2-yAl_2Si_2-yO_6$	(Holland and Powell, 1996)
Plagioclase (Plg)	$Na_xCa_{1-x}Al_2Si_2-xO_8$	(Newton et al., 1980)

The position of the solidus was computed using (White et al., 2001).

Additional mineral abbreviations: Quartz (Q), Lawsonite (Law), Albite (Ab), sillimanite (Sil), end-member Albite (Ab), Garnet (Gar), Clinopyroxene (Cpx), Jadeite (Jd), Epidote (Ep), Paragonite (Par), Amphibole (Amp), Corundum (Cor).

APPENDICES BIBLIOGRAPHY

Akinfiev, N., Zotov, A., 1999. Thermodynamic description of equilibria in mixed fluids (H₂O-non-polar gas) over a wide range of temperature (25–700°C) and pressure (1–5000 bars). *Geochimica et Cosmochimica Acta* 63, 2025–2041.

Anderson, G.M., Castet, S., Schott, J., Mesmer, R.E., 1991. The density model for estimation of thermodynamic parameters of reactions at high temperatures and pressures. *Geochimica et Cosmochimica Acta* 55, 1769–1779.

Anderson, G.M., Crerar, D.A., 1993. *Thermodynamics in geochemistry: The equilibrium model*. Oxford University Press.

Auzanneau, E., Schmidt, M.W., Vielzeuf, D., Connolly, J.D., 2010. Titanium in phengite: a geobarometer for high temperature eclogites. *Contributions to Mineralogy and Petrology* 159, 1–24.

Bandura, A.V., Lvov, S.N., 2006. The ionization constant of water over wide ranges of temperature and density. *Journal of Physical and Chemical Reference Data* 35, 15–30.

Benson, S., 1968. *Thermochemical Kinetics*. John Wiley and Sons.

Berman, R.G., 1988. Internally-Consistent Thermodynamic Data for Minerals in the System Na₂O-K₂O-CaO-MgO-FeO-Fe₂O₃-Al₂O₃-SiO₂-TiO₂-H₂O-CO₂, pp. 445–522.

Berman, R.G., Aranovich, L.Y., 1996. Optimized standard state and solution properties of minerals. *Contributions to Mineralogy and Petrology* 126, 1–24.

Berman, R.G., Brown, T., Greenwood, H.J., Greenwood, H.J., Pétrographe, S., Greenwood, H.J., Petrographer, S., 1985. An internally consistent thermodynamic data base for minerals in the system Na₂O-K₂O-CaO-MgO-FeO-Fe₂O₃-Al₂O₃-SiO₂-TiO₂-H₂O-CO₂. Atomic Energy of Canada.

Botti, A., Bruni, F., Mancinelli, R., Ricci, M.A., Lo Celso, F., Triolo, R., Ferrante, F., Soper, A.K., 2008. Study of percolation and clustering in supercritical water-CO₂ mixtures. *The Journal of Chemical Physics* 128, -.

Coggon, R., Holland, T.J.B., 2002. Mixing properties of phengitic micas and revised garnet-phengite thermobarometers. *Journal of Metamorphic Geology* 20, 683–696.

Connolly, J., 1995. Phase diagram methods for graphitic rocks and application to the system C–O–H–FeO–TiO₂–SiO₂. *Contributions to Mineralogy and Petrology* 119, 94–116.

Connolly, J.A.D., 1990. Multivariable phase diagrams; an algorithm based on generalized thermodynamics. *American Journal of Science* 290, 666–718.

Connolly, J.A.D., Cesare, B., 1993. C–O–H–S fluid composition and oxygen fugacity in graphitic metapelites. *Journal of Metamorphic Geology* 11, 379–388.

Dandurand, J.L., Schott, J., 1992. Prediction of ion association in mixed-crystal fluids. *The Journal of Physical Chemistry* 96, 7770–7777.

Davies, C.W., 1962. *Ion association*. Butterworths London.

de Santis, R., Breedveld, G., Prausnitz, J.M., 1974. Thermodynamic properties of aqueous gas mixtures at advanced pressures. *Industrial & Engineering Chemistry Process Design and Development* 13, 374–377.

Debye, P., 1929. *Polar molecules*. New York: Chemical Catalog Co., Inc.

Deul, R., Franck, E., 1991. The Static Dielectric Constant of the Water-Benzene Mixture System to 400° C and 2800 bar. *Berichte der Bunsengesellschaft für physikalische Chemie* 95, 847–853.

Dolejš, D., 2013. Thermodynamics of aqueous species at high temperatures and pressures: equations of state and transport theory. *Reviews in Mineralogy and Geochemistry* 76, 35–79.

Dubessy, J., Moissette, A., Bakker, R.J., Frantz, J.D., Zhang, Y.G., 1999. High-temperature Raman spectroscopic study of H₂O-CO₂-CH₄ mixtures in synthetic fluid inclusions; first insights on molecular interactions and analytical implications. *European Journal of Mineralogy* 11, 23–32.

Ehrenson, S., 1987. Boundary continuity and analytical potentials in continuum solvent models. Implications for the Born model. *The Journal of Physical Chemistry* 91, 1868–1873.

Facq, S., Daniel, I., Montagnac, G., Cardon, H., Sverjensky, D.A., 2014. In situ Raman study and thermodynamic model of aqueous carbonate speciation in equilibrium with aragonite under subduction zone conditions. *Geochimica et Cosmochimica Acta* 132, 375–390.

Haar, L., 1984. *NBS/NRC steam tables*. CRC Press.

Harvey, A.H., Lemmon, E.W., 2005. Method for estimating the dielectric constant of natural gas mixtures. *International Journal of Thermophysics* 26, 31–46.

Harvey, A.H., Prausnitz, J.M., 1987. Dielectric constants of fluid mixtures over a wide range of temperature and density. *J Solution Chem* 16, 857–869.

Helgeson, H., Delany, J., Nesbitt, H., D., B., 1978. Summary and critique of the thermodynamic properties of rockforming minerals. *Am. J. Sci* A 278, 229.

Helgeson, H.C., Kirkham, D.H., 1974. Theoretical prediction of the thermodynamic behavior of aqueous electrolytes at high pressures and temperatures; II, Debye-Huckel parameters for activity coefficients and relative partial molal properties. *American Journal of Science* 274, 1199–1261.

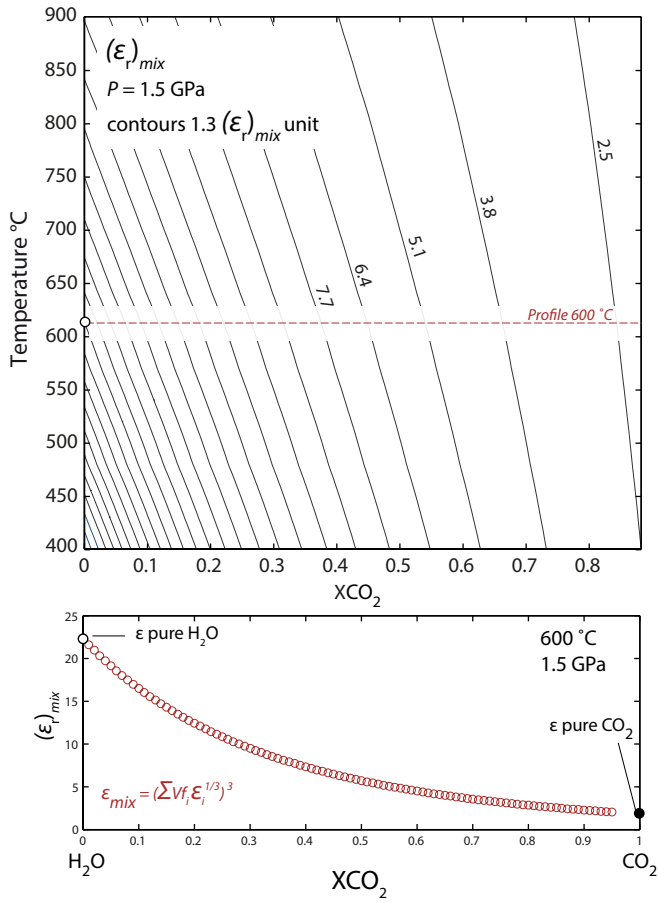
Helgeson, H.C., Kirkham, D.H., 1976. Theoretical prediction of the thermodynamic properties of aqueous electrolytes at high pressures and temperatures. III. Equation of state for aqueous species at infinite dilution. *American Journal of Science* 276, 97–240.

Helgeson, H.C., Kirkham, D.H., Flowers, G.C., 1981. Theoretical prediction of the thermodynamic behavior of aqueous electrolytes by high pressures and temperatures; IV, Calculation of activity coefficients, osmotic coefficients, and apparent molal and standard and relative partial molal properties to 600 degrees C and 5kb. *American Journal of Science* 281, 1249–1516.

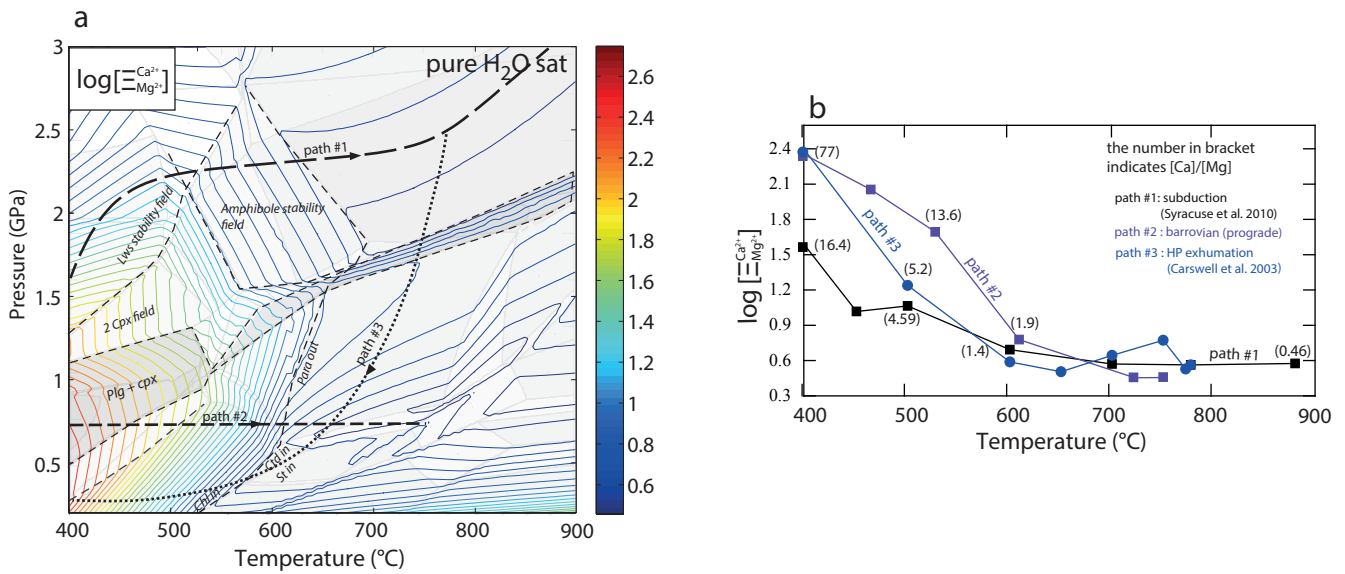
Holland, T., Baker, J., Powell, R., 1998. Mixing properties and activity-composition and relationships of chlorites in the system MgO-FeO-Al₂O₃-SiO₂-H₂O. *E. Schweizerbart'sche Verlagsbuchhandlung Science Publishers*, pp. 395–406.

Holland, T., Powell, R., 1991. A Compensated-Redlich-Kwong (CORK) equation for volumes and fugacities of CO₂ and H₂O in the range 1 bar to 50 kbar and 100–1600°C. *Contributions to Mineralogy and Petrology* 109, 265–273.

- Holland, T., Powell, R., 1996. Thermodynamics of order-disorder in minerals: II. Symmetric formalism applied to solid solutions. *American Mineralogist* 81, 1425-1437.
- Holland, T., Powell, R., 1998. An internally consistent thermodynamic data set for phases of petrological interest. *Journal of Metamorphic Geology* 16, 309-343.
- Holland, T.J.B., Powell, R., 2011. An improved and extended internally consistent thermodynamic dataset for phases of petrological interest, involving a new equation of state for solids. *Journal of Metamorphic Geology* 29, 333-383.
- Holloway, J., 1977. Fugacity and Activity of Molecular Species in Supercritical Fluids, in: Fraser, D. (Ed.), *Thermodynamics in Geology*. Springer Netherlands, pp. 161-181.
- Jacobs, G.K., Kerrick, D.M., 1981. Methane: An equation of state with application to the ternary system H₂O-CO₂-CH₄. *Geochimica et Cosmochimica Acta* 45, 607-614.
- Johnson, J.W., Oelkers, E.H., Helgeson, H.C., 1992. SUPCRT92: A software package for calculating the standard molal thermodynamic properties of minerals, gases, aqueous species, and reactions from 1 to 5000 bar and 0 to 1000°C. *Computers & Geosciences* 18, 899-947.
- Kirkwood, J.G., 1939. The dielectric polarization of polar liquids. *The Journal of Chemical Physics* 7, 911-919.
- Landau, L.D., Lifshitz, M., 1960. *Electrodynamics of Continuous Media*. Pergamon Press, Oxford.
- Looyenga, H., 1965. Dielectric constants of heterogeneous mixtures. *Physica* 31, 401-406.
- Mahar, E.M., Baker, J.M., Powell, R., Holland, T.J.B., Howell, N., 1997. The effect of Mn on mineral stability in metapelites. *Journal of Metamorphic Geology* 15, 223-238.
- Newton, R.C., Charlu, T.V., Kleppa, O.J., 1980. Thermochemistry of the high structural state plagioclases. *Geochimica et Cosmochimica Acta* 44, 933-941.
- Onsager, L., 1936. Electric moments of molecules in liquids. *Journal of the American Chemical Society* 58, 1486-1493.
- Oster, G., 1946. The Dielectric Properties of Liquid Mixtures. *Journal of the American Chemical Society* 68, 2036-2041.
- Pan, D., Spanu, L., Harrison, B., Sverjensky, D.A., Galli, G., 2013. Dielectric properties of water under extreme conditions and transport of carbonates in the deep Earth. *Proceedings of the National Academy of Sciences of the United States of America* 110, 6646-6650.
- Pérez-Salado Kamps, Á., 2005. Model for the Gibbs Excess Energy of Mixed-Solvent (Chemical-Reacting and Gas-Containing) Electrolyte Systems. *Industrial & Engineering Chemistry Research* 44, 201-225.
- Redlich, O., Kwong, J.N., 1949. On the thermodynamics of solutions. V. An equation of state. Fugacities of gaseous solutions. *Chemical reviews* 44, 233-244.
- Shock, E.L., Helgeson, H.C., 1988. Calculation of the thermodynamic and transport properties of aqueous species at high pressures and temperatures: Correlation algorithms for ionic species and equation of state predictions to 5 kb and 1000°C. *Geochimica et Cosmochimica Acta* 52, 2009-2036.
- Shock, E.L., Oelkers, E.H., Johnson, J.W., Sverjensky, D.A., Helgeson, H.C., 1992. Calculation of the thermodynamic properties of aqueous species at high pressures and temperatures. Effective electrostatic radii, dissociation constants and standard partial molal properties to 1000 °C and 5 kbar. *Journal of the Chemical Society, Faraday Transactions* 88, 803-826.
- Shock, E.L., Sassani, D.C., Willis, M., Sverjensky, D.A., 1997. Inorganic species in geologic fluids: correlations among standard molal thermodynamic properties of aqueous ions and hydroxide complexes. *Geochimica et Cosmochimica Acta* 61, 907-950.
- Sverjensky, D.A., Harrison, B., Azzolini, D., 2014. Water in the deep Earth: The dielectric constant and the solubilities of quartz and corundum to 60kb and 1200° C. *Geochimica et Cosmochimica Acta* 129, 125-145.
- Sverjensky, D.A., Hemley, J., d'Angelo, W., 1991. Thermodynamic assessment of hydrothermal alkali feldspar-mica-aluminosilicate equilibria. *Geochimica et Cosmochimica Acta* 55, 989-1004.
- Sverjensky, D.A., Shock, E.L., Helgeson, H.C., 1997. Prediction of the thermodynamic properties of aqueous metal complexes to 1000°C and 5 kb. *Geochimica et Cosmochimica Acta* 61, 1359-1412.
- Tajmanova, L., Connolly, J.A.D., Cesare, B., 2009. A thermodynamic model for titanium and ferric iron solution in biotite. *Journal of Metamorphic Geology* 27, 153-165.
- Tanger, J.C., Helgeson, H.C., 1988. Calculation of the thermodynamic and transport properties of aqueous species at high pressures and temperatures; revised equations of state for the standard partial molal properties of ions and electrolytes. *American Journal of Science*, pp. 19-98.
- Waldbaum, D.R., Thompson, J.B., 1968. Mixing properties of sanidine crystalline solutions. 2. Calculations based on volume data. *American Mineralogist* 53, 2000-2017.
- Walther, J.V., 1992. Ionic association in H₂O-CO₂ fluids at mid-crustal conditions. *Journal of Metamorphic Geology* 10, 789-797.
- Walther, J.V., Schott, J., 1988. The dielectric constant approach to speciation and ion pairing at high temperature and pressure.
- White, R.W., Powell, R., Holland, T.J.B., 2001. Calculation of partial melting equilibria in the system Na₂O-CaO-K₂O-FeO-MgO-Al₂O₃-SiO₂-H₂O (NCKFMASH). *Journal of Metamorphic Geology* 19, 139-153.
- White, R.W., Powell, R., Holland, T.J.B., Worley, B.A., 2000. The effect of TiO₂ and Fe₂O₃ on metapelitic assemblages at greenschist and amphibolite facies conditions: mineral equilibria calculations in the system K₂O-FeO-MgO-Al₂O₃-SiO₂-H₂O-TiO₂-Fe₂O₃. *Journal of Metamorphic Geology* 18, 497-512.
- Wolery, T.J., 1992. EQ3/6, a software package for geochemical modeling of aqueous systems: package overview and installation guide (version 7.0).
- Zhang, Z., Duan, Z., 2005. Prediction of the PVT properties of water over wide range of temperatures and pressures from molecular dynamics simulation. *Physics of the Earth and Planetary Interiors* 149, 335-354.

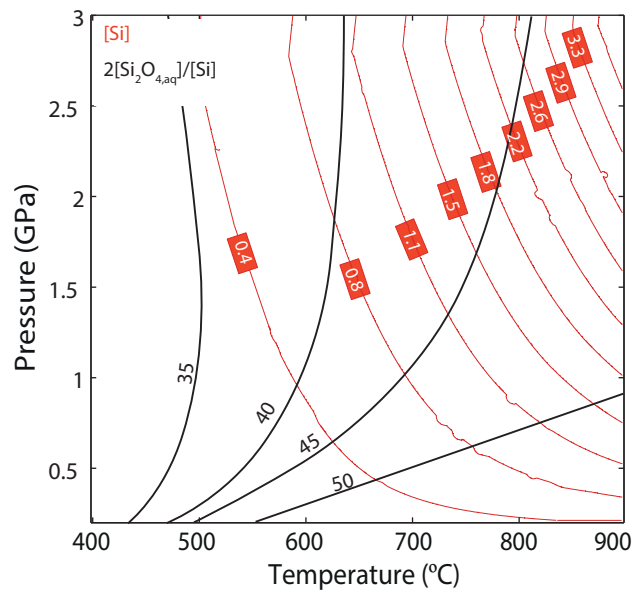


SOM Fig. 1. Relative permittivity of H_2O - CO_2 mixtures at 1.5 GPa. The mixing rule used here is from Looyenga (1965), and the volume fraction of H_2O - CO_2 are derived from a method as described in Harvey and Prausnitz (1989).

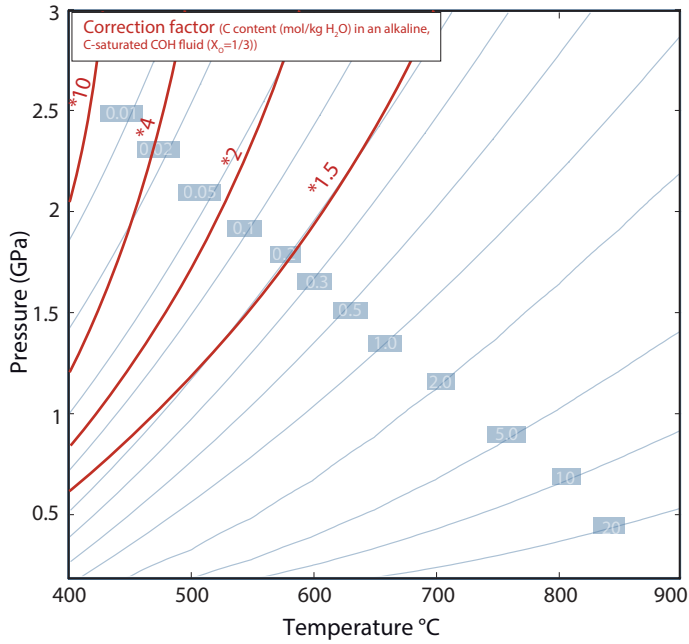


SOM Fig. 2. **a**. Contours of $\left[\Sigma_{Mg^{2+}}^{Ca^{2+}}\right]$ for model #1 **b**. Profile along three P - T paths for the ratio $\left[\Sigma_{Mg^{2+}}^{Ca^{2+}}\right]$. The corresponding ratio [Ca]/[Mg] is indicated in parenthesis. Panel (a.) shows a progressive but pronounced up- T decrease in $\Sigma_{Mg^{2+}}^{Ca^{2+}}$ from *ca.* 1.7 at low P and T , to *ca.* 0.6 at high T irrespective of the pressure. This general decrease tracks the destabilization, with rising T , of chlorite (at low P), paragonite (intermediate P), and glaucophane-rich amphibole (high P) (Fig. 4). At *ca.* 500 °C and with increasing P , $\Sigma_{Mg^{2+}}^{Ca^{2+}}$ decreases as lawsonite abundance increases. Values of $\Sigma_{Mg^{2+}}^{Ca^{2+}}$ display simple changes along the example P - T paths (Fig. 6b). The steady decrease in $\Sigma_{Mg^{2+}}^{Ca^{2+}}$ with rising T indicates that high $a(Ca^{2+})$ relative to $a(Mg^{2+})$ may be characteristic of low P - T environments, whereas higher $a(Mg^{2+})$ relative to $a(Ca^{2+})$ occurs over a broad range of high metamorphic P and T

Figure 6 Galvez et al.



SOM Fig. 3 Total silicon content in the equilibrium fluid (model#1) [Si] (molal) and fraction of dimer $2[\text{Si}_2\text{O}_{4,\text{aq}^-}]/[\text{Si}]$.



SOM Fig. 4 Contours of the correction factor returning [C] in the equilibrium fluid (model#2), *i.e.* corresponding to pH about 2 log units above neutrality (see Fig. 7a), and including species such as HCO_3^- , compared to values obtained from Connolly and Cesare (1993) (Fig. 2, and pale blue in the background). At elevated P and low T , *i.e.* in the blueschist-lawsonite metamorphic facies (upper left quadrant, see also Fig. 4), [C] in model #2 peaks at ca. 0.1 molal. Note that these results assume the chemical potentials of COH components (H_2O , CO_2 , CH_4 , H_2 , CO) are those returned by applying the EoS of Connolly and Cesare (1993) at all conditions, irrespective of the pH considered. The validity of this assumption is likely to be restricted to limited pH fluctuations (mostly alkalinization) around the slightly acidic values produced by equilibration of H_2O and elemental C (0.1 to 0.5 log units below neutral pH (pH_w^{mid} see text for details), as is the case here.